"In presenting the dissertation as a partial fulfillment of the requirements for an advanced degree from the Georgia Institute of Technology, I agree that the Library of the Institution shall make it available for inspection and circulation in accordance with its regulations governing materials of this type. I agree that permission to copy from, or to publish from, this dissertation may be granted by the professor under whose direction it was written, or such copying or publication is solely for scholarly purposes and does not involve potential financial gain. It is understood that any copying from, or publication of, this dissertation which involves potential financial gain will not be allowed without written permission.

_____

_____

AN INVESTIGATION OF FRICTION COEFFICIENTS IN THE INLET LENGTH OF A SMOOTH ROUND TUBE

A THESIS

Presented to

the Faculty of the Graduate Division

By

Leonard Hinson Taylor

In Partial Fulfillment

of the Requirements for the Degree

Master of Science in Mechanical Engineering

Georgia Institute of Technology

June 1955

AN INVESTIGATION OF FRICTION COEFFICIENTS

IN THE INLET LENGTH OF A SMOOTH ROUND TUBE

Approved:

Date Approved by Chairman: 3 May 1955

TABLE OF CONTENTS

LIST OF TABLES

LIST OF ILLUSTRATIONS

*Figures 1 through 21 refer to graphs of ratios of local and integrated apparent friction coefficients to the Karman-Nikuradse friction coefficient versus L/D ratios for the test indicated.

LIST OF ILLUSTRATIONS (Continued)

SYMBOLS

D	tube diameter, feet
ΔP	pressure drop between taps, inches of water
f_{APP}	apparent friction coefficient, dimensionless
$\bar{f}_{APP}$	integrated apparent friction coefficient, dimensionless
f_{K-N}	Karman-Nikuradse coefficient, dimensionless
L/D	ratio of distance from inlet to tube diameter
P	static pressure, feet of water
P_{cc}	pressure in calming chamber, pressure pounds per square inch gage
psig	pressure pounds per square inch gage
R_D	Reynolds number based on tube diameter, dimensionless
R_X	Reynolds number based on distance from tube inlet, dimensionless
T_w	temperature of water flowing through apparatus, °F
W_w	weight of water flowing through apparatus, pounds per minute
V	mean velocity based on mass rate of flow, feet per second
X	distance from tube inlet, feet
μ	viscosity, slugs per foot-second
ρ	density, slugs per cubic foot

SUMMARY

An experimental investigation was made of apparent friction coefficients in the inlet length of a smooth round tube with bellmouth entrances of different radii. Tests were conducted with flow of water through one-half inch copper tubing at Reynolds numbers varying from 29,400 to 149,500.

The results were recorded in terms of the local apparent friction coefficient and the integrated apparent friction coefficient. The apparent friction coefficient is a direct measure of the pressure loss and includes the effects of both friction and momentum flux changes. The integrated value of the coefficient is simply a measure of the total loss from the tube inlet to the point concerned.

The tests indicated that for a bellmouth entrance with a radius of one pipe diameter, the boundary layer was initially laminar with a transition to turbulent boundary layer at an average Reynolds number (based on distance from the tube inlet) of about 500,000. This value compares well with the corresponding value for a flat plate. The tests for the bellmouth entrances with radii of two and three pipe diameters indicated that an undetermined amount of turbulence existed at the tube inlet. This induced turbulence greatly affected the boundary layer and the friction coefficients within the inlet length. The initial turbulence caused the boundary layer to be turbulent from the beginning of the inlet length. The entrance with a radius of three pipe diameters caused more turbulence than the entrance with a radius of two pipe diameters.

Within the inlet length, the local apparent friction coefficient was found to vary widely from the Karman-Nikuradse coefficient for fully developed turbulent flow. The variations of the coefficient consisted of an initial decrease within the region of laminar boundary layer, an increase accompanying the transition to a turbulent boundary layer, a second decrease and fluctuations probably due to adjustments in velocity profiles. The initial decrease and increase were absent in the tests for which no laminar boundary layer existed. Also, elimination of the laminar boundary layer by induced turbulence acted to greatly increase the value of the friction coefficient in the region which would normally be the laminar inlet zone.

The experimental results for the tube with the bellmouth entrance with a radius of one pipe diameter tend to be in general agreement with the results of a similar investigation conducted by Shapiro and Smith and published in N.A.C.A. Technical Note #1785.

CHAPTER I

INTRODUCTION

Object.--The object of this investigation was to determine experimentally the values of apparent friction coefficients in the inlet length of round smooth tubes and to find the effect on the friction coefficient of the Reynolds number and the distance from the entrance. It was anticipated that the results of the tests, conducted with the flow of water at Reynolds numbers corresponding to fully developed turbulent flow, would supplement the results obtained by Shapiro and Smith in a similar investigation completed in 1947.

Survey of Literature.--When a fluid from a calm source flows steadily through a horizontal tube of uniform diameter, the velocity profile in the region downstream from the entrance varies with the distance from the entrance. After some distance downstream, the variations in the flow pattern disappear and the velocity profile remains unchanged. This length in which the flow pattern is developing is known as the "length of transition" or the "inlet length".

The changes in velocity profile in the inlet length have an important effect upon the friction coefficients in this region. It has been found that the friction coefficient varies considerably with distance from the inlet in the initial part of the inlet length. After the inlet length, the friction coefficient is constant and is independent of the

distance from the tube inlet. Values of the friction coefficients for the fully developed region have been established with accuracy through the efforts of many investigators. For the inlet length there is little data available.

The usual procedure for calculating friction coefficients from pressure loss data is based on the assumption that the velocity profile is constant at each cross section. Within the inlet length this procedure does not consider the momentum flux changes accompanying the velocity profile changes, and, therefore, the resulting friction coefficient does not represent the true drag coefficient. Friction coefficients in the inlet length that are calculated from pressure loss data are designated "apparent friction coefficients". The true friction coefficient or the ratio of the wall shearing stress to the velocity head is equal to the "apparent friction coefficient" only when the velocity profile is constant in all cross sections and the flow is incompressible. In order to calculate the values of true friction coefficient within the inlet length, it would be necessary to measure the changes in velocity profile.

Boussinesq (1), in 1890, obtained a solution for the development of the velocity profile for laminar flow. From his results it was concluded that for purely laminar flow, the length of transition in terms of a length-diameter ratio was

$$L/D = 0.065\ R_D$$

Schiller (2), in an investigation of laminar flow, assumed that the typical velocity profile near the inlet was composed of a straight line segment terminated by parabolic arcs. He then applied Karman's momentum

equation to the entire cross section and the Bernoulli equation to the central core of fluid. The rate of development of the velocity profile was computed and the pressure drop from the inlet predicted. For the length of transition, Schiller obtained the ratio

$$L/D = 0.029\ R_D$$

Langhaar (3) completed an analysis for laminar flow by employing a linearizing technique with the Navier-Stokes equation and retaining more terms than previous investigators. He assumed that the velocity was constant over the entire inlet cross section; tests by Nikuradse indicate that this assumption is justified for tubes with short bell mouthed entries. No definite inlet length was found, but the velocity profile was found to approach the parabolic form in asymptotic fashion. The length in which the center-line velocity reaches 99 percent of its asymptotic value was predicted to be

$$L/D = 0.115\ R_D$$

Latzko (4) analyzed the development of a turbulent velocity profile by assuming that a typical velocity profile in the inlet length is composed of a straight line segment terminated by arcs, the velocity distribution of which follows the one-seventh power law. From this he predicted the total inlet length of a purely turbulent flow to be

$$L/D = 0.69 R_D^{0.25}$$

Experimental investigations seem to have been limited in number and scope.

Kirsten (5) measured velocity profiles at various distances from bellmouth entrances for the flow of air through smooth tubes. His results indicated that the boundary layer near the entrance was initially laminar with a change to the type of combined laminar and turbulent boundary layer associated with flow over a flat plate and with a fully developed turbulent pipe flow.

Egli (6) investigated the flow of steam and air through narrow channels. He found that the friction coefficient was a function of the length-clearance ratio as well as the Reynolds number and the roughness. For flow through a channel of a fixed clearance, the friction coefficient decreased with an increase of the length-clearance ratio.

Keenan and Newmann (7) investigated the apparent friction coefficients for the flow of air through smooth pipes at subsonic and supersonic velocities. The air streams entered the tubes through bellmouth entrances. Results of this investigation led to the conclusion that within an entry length of about 50 diameters, the apparent friction coefficient for supersonic flow was a function of the length-diameter ratio and the Reynolds number. At distances from the inlet of greater than 50 diameters, it was found that the apparent friction coefficient for either subsonic or supersonic flow was approximately equal to the coefficients for incompressible flow with fully developed boundary layer. It was concluded that the variation of the friction coefficient with the length-diameter ratio at supersonic flow was similar to the variation corresponding to incompressible flow. The investigators agreed that an accurate comparison could not be made because insufficient data were available for incompressible flow through the inlet length.

Shapiro and Smith (8) investigated the apparent friction coefficients in the inlet length of smooth, round tubes with bellmouth entrances. The tests were conducted with water and air flowing at Reynolds numbers corresponding to fully developed turbulent flow. Values of the coefficients from these tests were reported in terms of local apparent friction coefficients and integrated apparent friction coefficients, the latter being a measure of the total pressure drop from the inlet to the point involved. Values of the local coefficient were compared with the Karman-Nikuradse coefficient for fully developed flow, the theory of Langhaar, and the flat plate theory.

The tests indicated that near the inlet there was a zone of laminar boundary layer, followed by a region in which the boundary layer was turbulent. Transition from laminar to turbulent boundary layer was found to occur at a Reynolds number based on distance from tube inlet of about 5×10^5, which compares well with the flat plate theory. The apparent friction coefficient in the laminar inlet zone varied approximately inversely as the 0.6 power of the distances from the inlet. A sharp rise in apparent friction coefficient accompanied the change from a laminar to a turbulent boundary layer. Near the beginning of the turbulent inlet zone there were rapid and irregular changes in the local apparent friction coefficient, followed by the coefficient approaching the Karman-Nikuradse coefficient.

Within the laminar inlet zone, the local apparent coefficient varied from 3.5 to 0.5 times the Karman-Nikuradse coefficient. The investigators were of the opinion that very near the inlet it was probable that the apparent friction coefficient was infinite as compared with the Karman-Nikuradse coefficient.

Values of the local apparent friction coefficient remained within 5 percent of the Karman-Nikuradse coefficient beginning at about 40 to 60 diameters from the tube inlet. The integrated apparent friction coefficient remained within 5 percent of the Karman-Nikuradse coefficient after 80 tube diameters from the tube inlet.

Huie (9) investigated the flow of water in the inlet length of smooth, round tubes with bellmouth entrances. His results agree in general with those of Shapiro and Smith.

The similarity between fluid friction and heat transfer has been pointed out by numerous investigators. Heat transfer in the inlet length should, therefore, compare with fluid friction in the same region.

White (10) analyzed the similarity between fluid friction and heat transfer for several cases, including the entry section of smooth round tubes. He suggested that for tubes with an abrupt entrance, the increased friction loss in the entry section can be considered by adding to the friction factor a quantity

$$f' = 0.4\ D/L$$

Aladyev (11) was concerned solely with heat transfer to water in the inlet length of tubes at various Reynolds numbers. From his tests he concluded that heat transfer is independent of the distance from the inlet for values of L/D greater than 40.

Boelter, Young, and Iverson (12) experimented with the heat transfer to air in the inlet length using various entry shapes before the test section. These tests showed that the heat transfer was affected by

the shape of the entry. An equation for heat transfer which they developed shows that the heat transfer rate is not affected by the distance from the inlet for values of L/D greater than $R^{0.25}$.

CHAPTER II

APPARATUS

A flow diagram of the apparatus used in this investigation is given in figure 25.

The water used for the tests was obtained from a line supplied by a centrifugal pump at approximately 60 psig. Water from the supply line passed through a globe valve, through the calming chamber to the test section, through a second globe valve, and was then discharged to an open weighing tank.

In order to obtain a condition of uniform velocity and minimum turbulence in the flow at the inlet to the test section, a calming chamber was placed upstream from the entrance to the test section. This calming chamber was a ten inch pipe four feet eight inches in length, with a baffle, tube bundle, and screens as shown in figure 27. The baffle was made of sheet brass with one-inch holes drilled so as to distribute the water uniformly over the entire cross section of the calming chamber. The tube bundle was made of two-foot lengths of one and one-quarter inch pipe filed smooth, painted for prevention of corrosion, and wired together to prevent movement. Two brass screens were installed downstream of the tube bundle to remove any turbulence caused by the tube bundle. It was believed that this arrangement of the calming chamber together with an area reduction with a ratio of greater than 300 to 1 would give substantially uniform flow approaching the test section.

The test section was attached to the calming chamber by a bellmouth entry section machined from brass to close tolerances. The same tube was used in all tests, but three different entry sections were used. In each case the inlet curve was a circular arc. The radii on the sections were one pipe diameter, two pipe diameters, and three pipe diameters. Each entry was attached to the test section with solder and the joint was burnished so that there was no observable roughness where the bellmouth and tube were connected.

The test section was made of one-half inch Type L hard drawn copper tubing approximately one hundred diameters in length. Pressure taps were located as indicated in table 22. Entry sections II and III had the first tap at the junction between the entry and the test section. Due to the construction of entry section I, it was not possible to have a tap at this position. The first tap with this entry section was one-half diameter downstream from the junction. The pressure taps were closely spaced near the entrance as it was felt that the greatest changes in velocity profile would occur in this region. The pressure taps were drilled through the tube walls and the inside of the tube was burnished to make sure that the tube wall was free of burrs. Connections were made to the pressure taps by means of one-quarter inch copper tubing soldered to the outside wall of the test section.

Each pressure tap was connected through copper tubing and shutoff valves to two pressure manifolds arranged so that any tap could be connected to either leg of three different manometers. Therefore, pressure differences between any two taps could be measured on any one of the manometers.

Also, the taps could be reversed relative to the manifolds and the manometers, thus affording a test for leakage.

The manometers used were a mercury-water U-tube manometer, a vertical air-water manometer, and an inclined air-water manometer. The last named manometer was inclined at an angle of 11° 32' (sine = 0.200). The air-water manometers were inverted U-tubes constructed so as to permit application of a common air pressure to the top of both legs. The water pressure manifolds were connected to the bottom of the manometer legs. Upon application of water pressure to the manometers, the water level would rise until the total head was equalized by the air pressure. The difference in height of the two columns of water thus indicated the pressure drop between taps. The air pressure applied to the manometers was controlled by a constant pressure valve.

CHAPTER III

TEST PROCEDURE

To initiate a test, the supply valve and the discharge valve were regulated to permit the approximate rate of flow desired. The water flowing through the apparatus was weighed by discharging into an open tank. After the approximate flow rate was established, air was purged from the system. The calming chamber was purged by means of a plug in the top of the chamber. Next, the pressure taps, manifolds, manometers, and all connecting tubing were purged. This was accomplished by removing a plug above the manometer, opening all valves, and permitting the water to flow for an adequate time through each manifold and through each leg of the air-water manometers. Air was purged from the lines to the water-mercury manometer by loosening the connections at the top of the manometer. After the air was purged, final adjustments were made to the water flow rate. This rate was checked by weighing the discharge for one minute. After all pressure readings were taken, the rate of flow was again checked. The difference in flow rate at the beginning and at the end of each test did not exceed one percent.

With two pressure tap shutoff valves open to opposite manifolds, air pressure was applied to the top of the air-water manometers, thus forcing the water level down into the legs of the manometer. Time was allowed for all water droplets to drain into the manometer, and all entrained air bubbles were removed from the water columns. Care was

taken to prevent the water level dropping and entraining air in the manifolds at the bottom of the manometers.

The details of the testing procedure varied with each test, but certain general principles were followed. The inclined air-water manometer was used in the tests where only small differences in pressure existed between taps. Larger pressure differences were measured with the vertical air-water manometer, with the water-mercury manometer being used for high rates of flow only on the taps downstream from twelve pipe diameters.

To measure the pressure drop between any two points, the taps were opened to opposite pressure manifolds by means of the shutoff valves. Then, by means of manometer shutoff valves, the manifolds were opened to opposite legs of the manometer being used. After observing the pressure difference, the taps were reversed relative to the legs of the manometer and a second value for the pressure drop was observed.

In order to maintain the accuracy of the observed data, the pressure drops were measured and recorded in an accumulative manner as far as possible. For example, pressure drops were measured between taps one and two, one and three, one and four, and so on until limited by the range of the manometer being used. In the same manner, subsequent downstream measurements were recorded relative to other selected taps. The equalization of air pressure and water pressure in the air-water manometers resulted in fluctuations of the water levels in the legs. All measurements were read from these manometers by two observers.

The pressure in the calming chamber was observed throughout the test and did not change. The temperature of the water flowing was measured frequently and did not change more than one-half degree during a test.

CHAPTER IV

DISCUSSION

The results of the test are given in figures 1 through 21 in the form of curves in which the ratios of the local apparent friction coefficient and the integrated apparent friction coefficients to the Karman-Nikuradse coefficient are plotted against the ratio of the distance from the inlet to the tube diameter. The results of each test were plotted in separate figures. In figures 22 through 24, values of the local apparent friction coefficient are plotted against values of R_X (Reynolds number based on distance from the inlet). For purposes of comparison, the values of friction coefficients according to the theory of Langhaar and the value according to the theory of laminar and turbulent flow over a flat plate are also plotted.

Entry I.—Figures 1 to 7 seem to show no regularity in the variation of the local apparent friction coefficient. In each of the tests, the friction coefficient ratio is near unity for the pressure drop between taps one and two. The ratio for the pressure drop between taps two and three then rises to values of between 1.43 and 2.04. This is followed in general by a series of smaller fluctuations, and then a sharp rise in the ratio. The location of this rise tends to be closer to the entry to the tube as the Reynolds number becomes larger.

The integrated-coefficient ratio is initially high, followed by a decrease to a value of approximately 1.0 and then a rise. This rise

reaches a maximum at a value of X/D that tends to be closer to the entry with increasing Reynolds numbers. Downstream from this maximum point, the ratio decreases. This ratio tends to approach closer to unity for the larger values of the Reynolds number.

In the investigation by Huie, the integrated friction coefficient ratio was indicated to be below 1.0 at several points of measurement when the same pipe size and entry section were used. This investigation shows the ratio to drop below 1.0 in only a few places, with the minimum value being 0.98. It is believed that the larger number of pressure readings tends to give a better indication of the values of the ratio.

In figure 22 the local apparent friction coefficient for three of the tests is plotted against the Reynolds number based on distance from the inlet. The value of the coefficients in general follows the theory of Langhaar to a value of R_X of from 4 to 6 x 10^5. After a transition region in which the friction coefficient rises sharply, the coefficient shows a general trend downward toward an asymptote. In the turbulent region the coefficients are roughly double the values for turbulent flow over a flat plate. The region in which the transition from laminar to turbulent flow takes place corresponds in general to the section of the pipe in which the integrated friction coefficient reaches a maximum following its initial decrease.

This series of tests does not indicate the value of X/D at which the inlet effects become negligible. However, it appears that the variations in the local apparent friction coefficient become much smaller after the pressure reading at 44 pipe diameters from the tube inlet. This

agrees in general with the results of Shapiro and Smith, and as pointed out by them these values of X/D are far smaller than those predicted by the laminar inlet theories of Boussinesq, Schiller, and Langhaar, and are about three times as large as the value predicted by the turbulent inlet theory of Latzko.

Boelter, Young, and Iverson developed equations for the transfer of heat in the transition length of a tube that indicated that the transition length is equal to the Reynolds number raised to the one-fourth power. According to this relation, the transition length would vary from an X/D value of 13.3 for test A to an X/D value of 19.5 for test G.

Entry II.--Figures 8 to 14 show the local apparent friction coefficient ratio and the integrated apparent friction coefficient ratio plotted against the x/D ratio. In tests A, B, C, and D the local apparent friction coefficient ratio at the first tap had a value of from 2.70 to 4.20. At the second tap the ratio had a value of from 0.0 to 2.68, and at the third tap the value of the ratio was from 4.80 to 12.2. At the fourth and fifth taps there was a rise in pressure along the length of the tube. In tests E, F, and G the ratio at the first tap was from 1.20 to 1.75, at the second tap was from 3.68 to 3.92, and at the third tap was from 4.38 to 4.75. In these tests there was also a rise in pressure at the fourth and fifth taps.

This rise in the local apparent coefficient ratio is similar to results in an investigation by Aladyev. He was measuring heat transfer to water in a tube, and found a variation in the pipe wall temperature similar to the above variation in pressure drop in the tube. No direct

comparison can be made, as Aladyev measured the pipe wall temperature in only three places near the entry and gave no details of the shape of the entry section.

The integrated apparent friction coefficient ratio reaches a maximum at an x/D ratio of 1.5. The friction ratio then fell off rapidly. For tests A, B, C, and D there were no large changes in the friction ratio past x/D of 2.5. In tests E, F, and G this change to more steady values did not occur until about x/D of 7.

In figure 23 the local apparent friction coefficient for three of the tests is plotted against the Reynolds number based on distance from the inlet. The value of the coefficients seems to indicate that the flow is turbulent for all the points plotted. The value of the friction coefficient at high Reynolds numbers appears to be about double the value of the friction for turbulent flow over a flat plate. For lower values of the Reynolds numbers, the friction coefficient tends to approach the flat plate friction more closely. The larger radius of the entry seemed to have the effect of moving the transition region nearer to the entry.

Entry III.—Figures 15 to 21 show the local apparent friction coefficient ratio and the integrated apparent friction coefficient ratio plotted against the x/D ratio. In all of these tests there is a large pressure drop at the first tap followed by a pressure rise. The number of taps that exhibit this pressure rise varies with the Reynolds number, there being five taps with a pressure rise in test A and only one tap with a pressure rise in test G.

The integrated apparent friction coefficient starts with a very high value and falls off rapidly. There were in general only small changes in the ratio after a value of x/D of 5. Boelter, Young, and Iverson found similar results for heat transfer to air passing through a tube when the entry was an ASME nozzle shape. In some of the tests, the heat transfer rate reached a minimum at an x/D value of 3 and then rose to a steady rate at an x/D value of 8. For higher values of the Reynolds number a test showed a high initial heat transfer rate with the rate dropping until a steady value was reached at an x/D value of 8.

In figure 24 the local apparent friction coefficient for three of the tests is plotted against the Reynolds number based on distance from the inlet. The value of the coefficients seems to indicate that the flow is turbulent for all the points plotted. There is a great similarity between figures 23 and 24, with entry III giving generally lower values of the friction coefficient than were obtained with entry II. This would seem to indicate that the turbulent region developed further upstream with entry III than with entry II.

This series of tests seems to indicate that the inlet effect becomes negligible at x/D values of between 5 and 8, increasing with increasing Reynolds numbers. This apparently agrees with the idea of Boelter, Young, and Iverson that the transition length is a function of the Reynolds number, varying about as the one-fourth power.

CHAPTER V

CONCLUSIONS

The following conclusions were drawn from the experimental investigation of friction coefficients in the inlet length of a smooth round tube with bellmouth entrances of different radii.

1. It is the opinion of the writer that the bellmouth entrance with a radius of one pipe diameter gave a substantially uniform velocity distribution at the tube inlet.

2. For flow through inlet I the boundary layer is at first laminar and subsequently becomes turbulent at a value of Reynolds number based on distance from the tube inlet of about 5×10^5, which is about the same as the corresponding value for a flat plate.

3. Within the region of the laminar boundary layer, the local apparent friction coefficient decreased with increasing distance from the tube inlet.

4. A sharp increase in the friction coefficient accompanied the transition from laminar to turbulent boundary layer.

5. The measured values of the local apparent friction coefficient support the laminar inlet theory of Langhaar.

6. For flow through inlets II and III the boundary layer was turbulent from the beginning of the inlet length.

7. Elimination of the laminar boundary layer acted to greatly increase the value of the apparent friction coefficient in the region which would normally be the laminar inlet zone.

8. No definite value of the inlet length could be accurately determined. Indications are that the length is less than that predicted by Langhaar.

CHAPTER VI

RECOMMENDATIONS

In the experimental investigations of the friction coefficients in the inlet length of round tubes, one of the problems appears to be that of having a uniform velocity distribution at the tube inlet. The investigations listed in the bibliography have generally assumed that a uniform velocity does exist at the tube inlet. Shapiro and Smith showed that this assumption of uniform velocity may be affected by the approach to the bellmouth entry. In the present investigation, the use of bellmouth entries with a large radius gave a less uniform velocity distribution than the bellmouth with a radius of one pipe diameter. Investigation is needed to find what combinations of approach and bellmouth radius will give the closest approach to a uniform entry velocity.

The water levels in the air-water manometers tended to fluctuate rather violently at times due partly to difficulty in balancing the air and water pressures. It is believed that an inverted two fluid manometer would give greater stability. The connecting lines to the manometer should be equipped with diaphragms to prevent loss of the lighter fluid during preliminary adjustments of the system.

APPENDIX A

EXPERIMENTAL RESULTS

Table 1. Test A, Entry I

P_{cc} 51 psig

W_w 51½ lbs/min.

T_w 58°

R_D 30,700

f_{K-N} 0.0234

Pressure Taps	ΔP ("H_2O)	f_{APP}	f_{APP}/f_{K-N}	$\bar{f}_{APP}$	$\bar{f}_{APP}/f_{K-N}$
1-2	.18	0.0272	1.16	0.0272	1.16
2-3	.31	0.0468	2.01	0.0371	1.59
3-4	.13	0.0196	.84	0.0310	1.32
4-5	.15	0.0226	.97	0.0291	1.24
5-6	.18	0.0272	1.17	0.0288	1.23
6-7	.16	0.0242	1.04	0.0280	1.20
7-8	.14	0.0212	.91	0.0270	1.15
8-9	.15	0.0226	.97	0.0264	1.13
9-10	.18	0.0272	1.17	0.0264	1.13
10-11	.15	0.0226	.97	0.0262	1.12
11-12	.12	0.0181	.77	0.0254	1.09
12-13	.12	0.0181	.77	0.0246	1.05
13-14	.15	0.0226	.97	0.0246	1.05
14-15	.11	0.0166	.71	0.0240	1.03
15-16	.18	0.0272	1.17	0.0243	1.04
16-17	.14	0.0212	.91	0.0241	1.03
17-18	.30	0.0453	1.94	0.0252	1.08
18-19	.19	0.0287	1.23	0.0254	1.09
19-20	.16	0.0242	1.04	0.0254	1.09
20-21	.15	0.0226	.97	0.0253	1.08
21-22	.27	0.0408	1.75	0.0259	1.11
22-23	.21	0.0317	1.36	0.0262	1.12
23-24	.29	0.0437	1.87	0.0270	1.15
24-25	1.37	0.0258	1.11	0.0268	1.14
25-26	2.83	0.0267	1.14	0.0267	1.14
26-27	2.62	0.0246	1.06	0.0262	1.12
27-28	3.88	0.0246	1.05	0.0256	1.09
28-29	5.20	0.0247	1.06	0.0254	1.08
29-30	5.16	0.0244	1.05	0.0254	1.08
30-31	6.10	0.0231	.99	0.0250	1.07

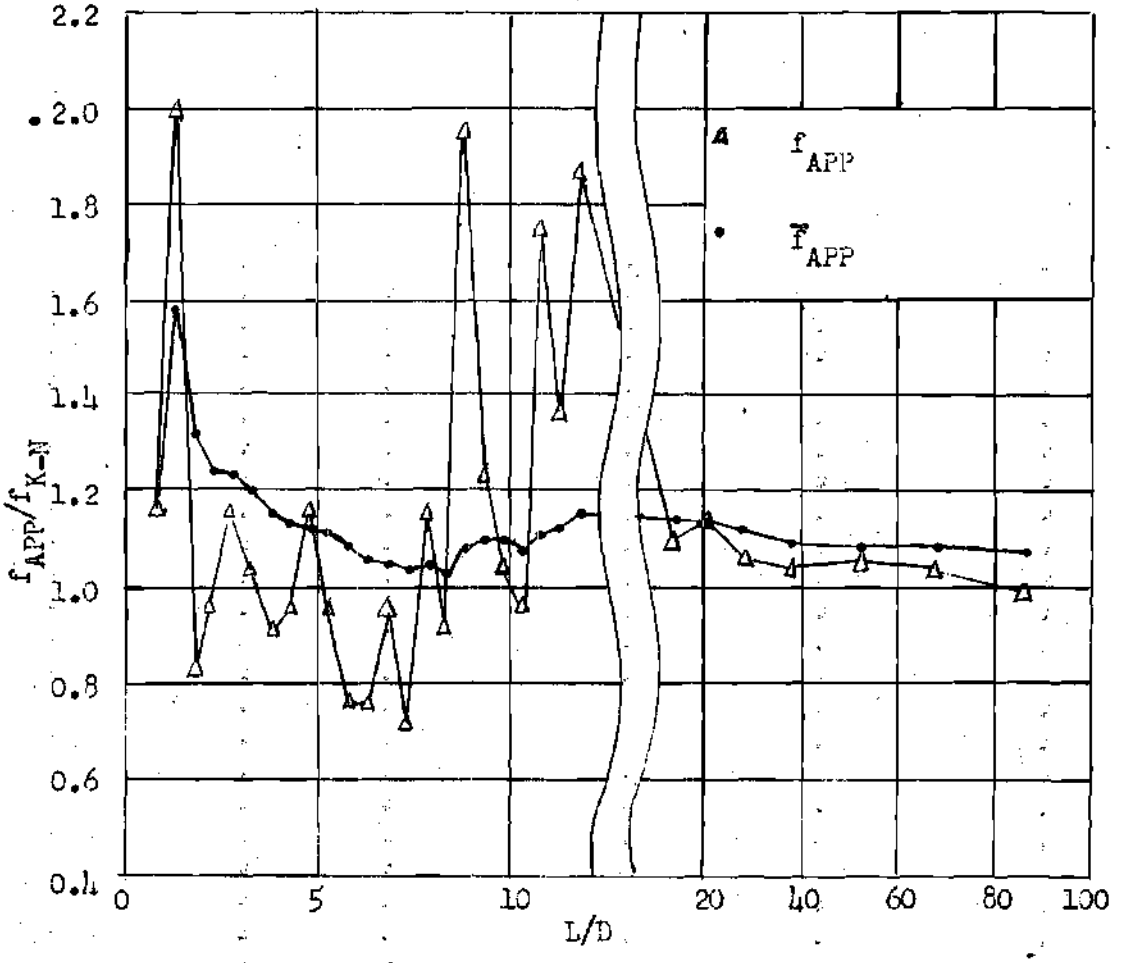

Figure 1. Results for Test A, Entry I. Ratios of local and integrated apparent friction coefficients to the Karman-Nikuradse friction coefficient against L/D for constant value of R_D.

Table 2. Test B, Entry I

P_{cc} 42 psig

W_w 91 lbs/min.

T_w 58°

R_D 53,800

f_{K-N} 0.0205

Pressure Taps	ΔP ($"H_2O$)	f_{APP}	f_{APP}/f_{K-N}	$\bar{f}_{APP}$	$\bar{f}_{APP}/f_{K-N}$
1-2	.38	.0212	1.04	.0212	1.04
2-3	.56	.0312	1.53	.0264	1.29
3-4	.42	.0234	1.14	.0254	1.24
4-5	.38	.0212	1.04	.0244	1.19
5-6	.28	.0156	.77	.0226	1.11
6-7	.36	.0200	.98	.0222	1.09
7-8	.36	.0200	.98	.0220	1.08
8-9	.35	.0195	.96	.0216	1.06
9-10	.35	.0195	.96	.0214	1.05
10-11	.36	.0200	.98	.0213	1.04
11-12	.34	.0190	.93	.0211	1.03
12-13	.54	.0301	1.47	.0218	1.06
13-14	.44	.0246	1.20	.0220	1.08
14-15	.31	.0173	.85	.0218	1.03
15-16	.52	.0290	1.42	.0222	1.08
16-17	.69	.0384	1.88	.0232	1.13
17-18	.27	.0151	.74	.0228	1.11
18-19	.45	.0251	1.23	.0229	1.12
19-20	.32	.0179	.88	.0226	1.10
20-21	.24	.0134	.66	.0221	1.08
21-22	.50	.0279	1.36	.0224	1.09
22-23	.60	.0334	1.63	.0230	1.12
23-24	.70	.0390	1.91	.0237	1.16
24-25	3.40	.0237	1.16	.0236	1.15
25-26	6.30	.0220	1.08	.0231	1.13
26-27	6.38	.0222	1.09	.0230	1.12
27-28	9.68	.0225	1.10	.0228	1.11
28-29	12.10	.0211	1.03	.0224	1.09
29-30	11.94	.0208	1.02	.0220	1.07
30-31	15.86	.0221	1.08	.0220	1.07

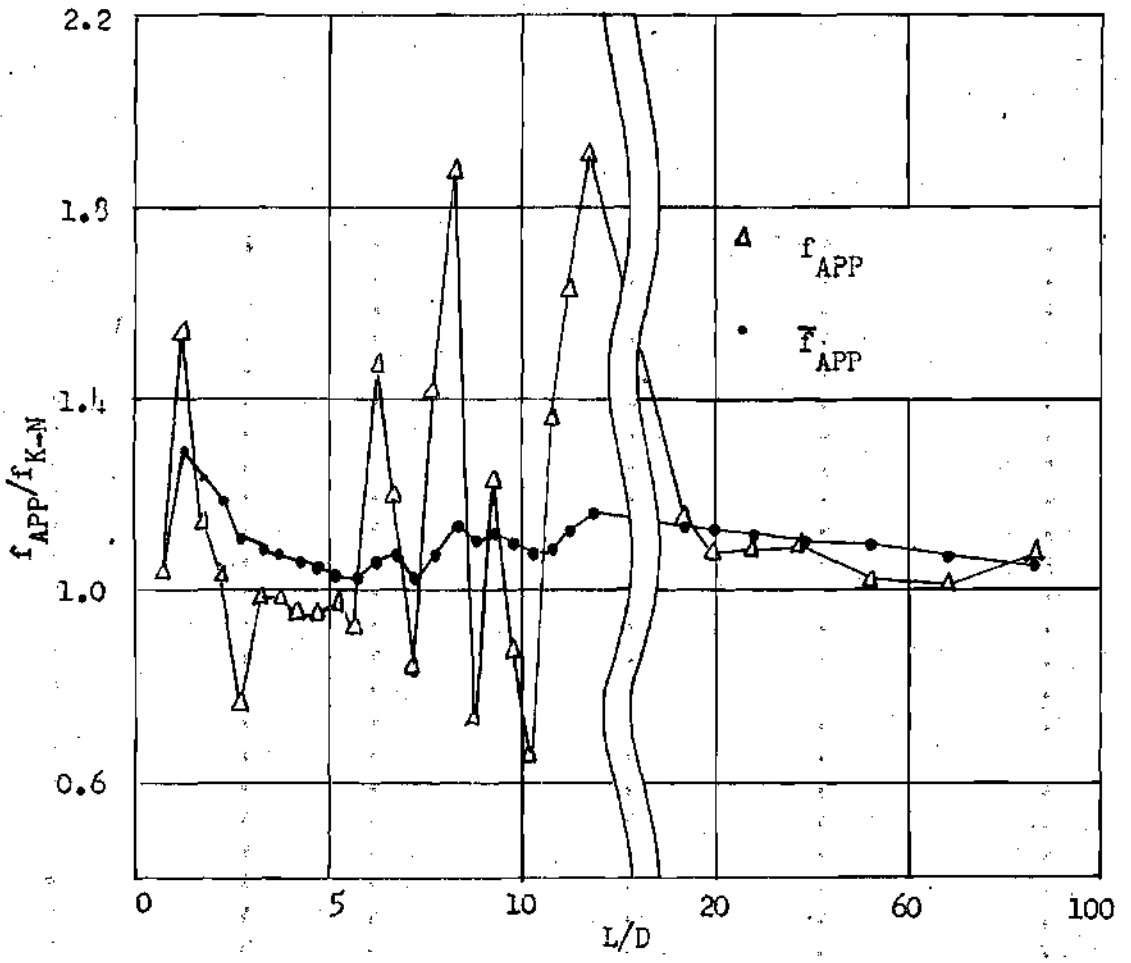

Figure 2. Results for Test B, Entry I. Ratios of local and integrated apparent friction coefficients to the Karman-Nikuradse friction coefficient against L/D for a constant value of R_D.

Table 3. Test C, Entry I

P_{cc} 34 psig

W_w 121 lbs/min.

T_w 57½°

R_D 72,900

f_{K-N} .0192

Pressure Taps	ΔP ("H_2O)	f_{APP}	f_{APP}/f_{K-N}	$\overline{f}_{APP}$	$\overline{f}_{APP}/f_{K-N}$
1-2	.71	.0192	1.0	.0192	1.0
2-3	1.31	.0354	1.85	.0272	1.42
3-4	.88	.0238	1.24	.0260	1.36
4-5	.62	.0168	.88	.0238	1.24
5-6	.73	.0197	1.03	.0230	1.20
6-7	.72	.0195	1.02	.0224	1.17
7-8	.78	.0211	1.10	.0222	1.16
8-9	.75	.0203	1.06	.0219	1.14
9-10	.55	.0149	.78	.0211	1.10
10-11	.36	.0097	.51	.0200	1.04
11-12	.57	.0154	.80	.0196	1.02
12-13	.51	.0138	.72	.0191	.99
13-14	.80	.0216	1.13	.0193	1.01
14-15	.59	.0159	.83	.0190	.99
15-16	1.61	.0435	2.27	.0207	1.08
16-17	1.17	.0316	1.65	.0214	1.12
17-18	.96	.0259	1.35	.0216	1.13
18-19	1.39	.0376	1.96	.0225	1.17
19-20	.47	.0127	.66	.0221	1.15
20-21	1.56	.0421	2.20	.0230	1.20
21-22	1.00	.0270	1.41	.0232	1.21
22-23	.98	.0264	1.38	.0233	1.21
23-24	.70	.0189	.99	.0232	1.21
24-25	6.1	.0206	1.08	.0224	1.17
25-26	10.6	.0179	.94	.0210	1.10
26-27	12.7	.0214	1.12	.0211	1.10
27-28	19.0	.0214	1.12	.0212	1.11
28-29	24.7	.0208	1.08	.0210	1.10
29-30	21.9	.0185	.96	.0206	1.07
30-31	30.8	.0208	1.08	.0205	1.07

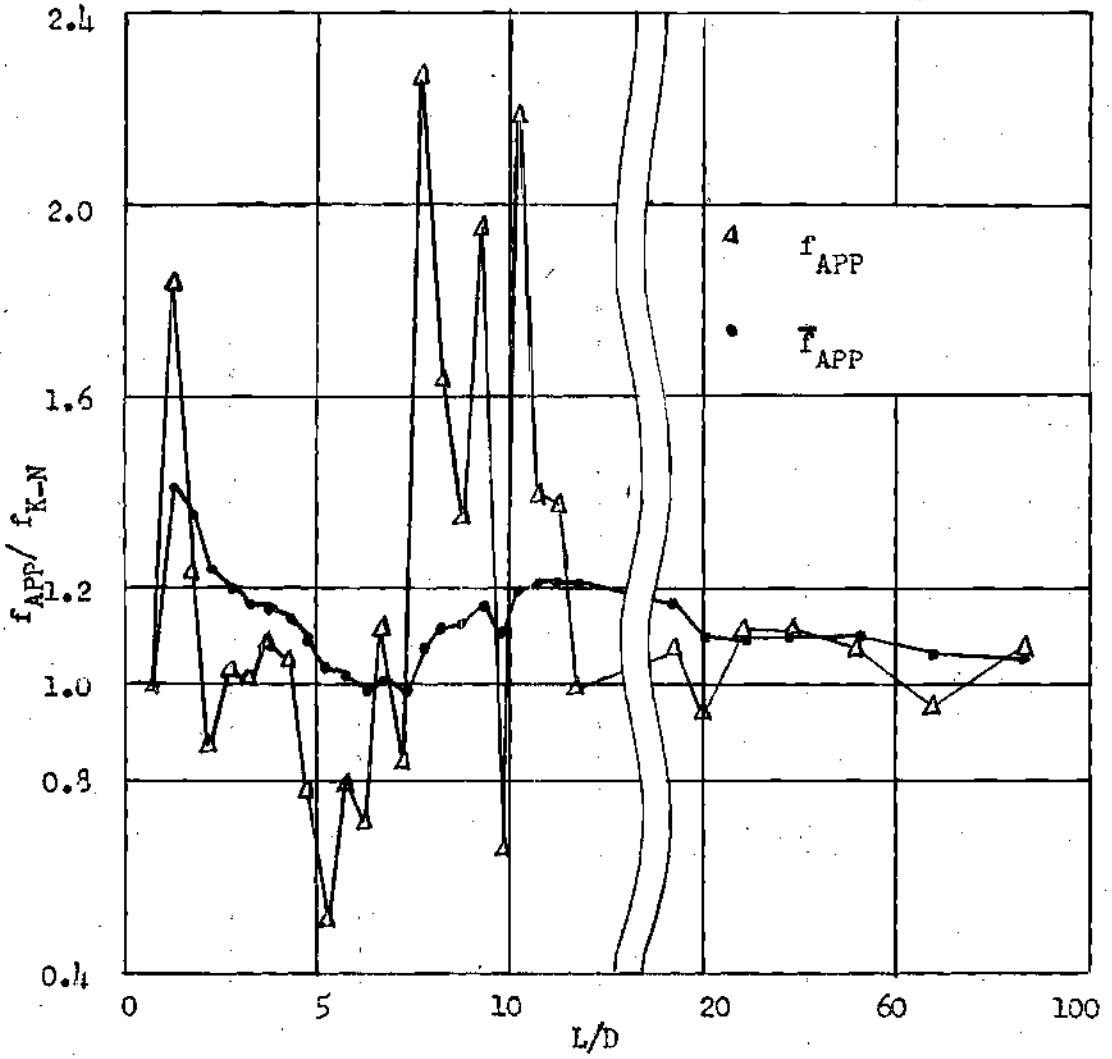

Figure 3. Results for Test C, Entry I. Ratios of local and integrated apparent friction coefficients to the Karman-Nikuradse friction coefficient against L/D for a constant value of R_D.

Table 4. Test D, Entry I

P_{cc} 30 psig

W_w 143 lbs/min.

T_w 53½°

R_D 86,000

f_{K-N} .0186

Pressure Taps	ΔP ($"H_2O$)	f_{APP}	f_{APP}/f_{K-N}	$\overline{f}_{APP}$	$\overline{f}_{APP}/f_{K-N}$
1-2	.94	.0182	.98	.0182	.98
2-3	1.96	.0378	2.04	.0282	1.52
3-4	.99	.0191	1.03	.0252	1.36
4-5	.32	.0062	.33	.0204	1.10
5-6	.78	.0151	.82	.0198	1.06
6-7	1.48	.0286	1.54	.0219	1.18
7-8	1.88	.0363	1.96	.0235	1.26
8-9	1.40	.0270	1.46	.0238	1.28
9-10	.34	.0066	.35	.0219	1.18
10-11	.57	.0110	.59	.0214	1.15
11-12	.30	.0058	.31	.0194	1.05
12-13	.83	.0160	.86	.0192	1.03
13-14	.45	.0087	.47	.0184	.99
14-15	1.13	.0218	1.17	.0184	.99
15-16	1.00	.0194	1.04	.0187	1.01
16-17	2.6	.0504	2.72	.0214	1.15
17-18	1.1	.0213	1.15	.0214	1.15
18-19	2.7	.0524	2.82	.0224	1.21
19-20	2.3	.0445	2.40	.0237	1.27
20-21	1.3	.0252	1.36	.0238	1.28
21-22	.7	.0135	.73	.0232	1.25
22-23	1.2	.0232	1.25	.0234	1.26
23-24	2.2	.0426	2.30	.0242	1.30
24-25	10.0	.0242	1.30	.0242	1.30
25-26	15.0	.0182	.98	.0220	1.18
26-27	17.5	.0212	1.14	.0218	1.17
27-28	25.3	.0204	1.10	.0215	1.16
28-29	29.3	.0177	.96	.0204	1.10
29-30	29.5	.0178	.96	.0198	1.06
30-31	36.5	.0176	.95	.0195	1.05

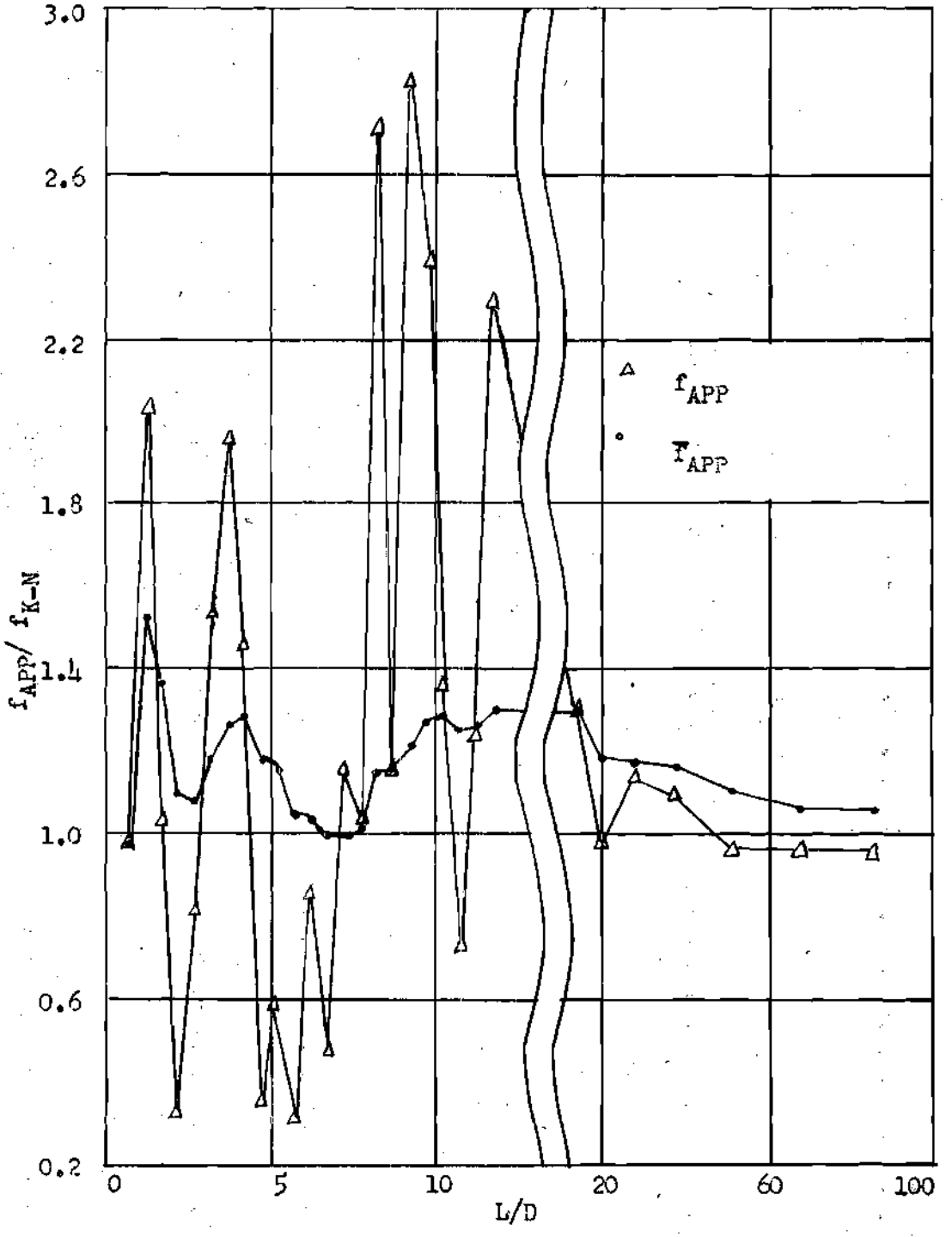

Figure 4. Results for Test D, Entry I. Ratios of local and integrated apparent friction coefficients to the Karman-Nikuradse friction coefficient against L/D for a constant value of R_D.

Table 5. Test E, Entry I

P_{cc} 32 psig

W_w 166 lbs/min.

T_w 53°

R_D 92,500

f_{K-N} .0183

Pressure Taps	ΔP ($"H_2O$)	f_{APP}	f_{APP}/f_{K-N}	$\bar{f}_{APP}$	$\bar{f}_{APP}/f_{K-N}$
1-2	1.3	.0187	1.02	.0187	1.02
2-3	1.99	.0286	1.57	.0236	1.29
3-4	1.19	.0171	.94	.0214	1.17
4-5	1.40	.0202	1.10	.0212	1.16
5-6	1.67	.0240	1.31	.0216	1.18
6-7	1.46	.0210	1.15	.0216	1.18
7-8	1.65	.0238	1.30	.0220	1.20
8-9	1.06	.0152	.83	.0210	1.15
9-10	1.00	.0144	.79	.0203	1.11
10-11	1.60	.0230	1.26	.0206	1.12
11-12	.60	.0086	.47	.0192	1.05
12-13	.60	.0086	.47	.0185	1.01
13-14	1.20	.0173	.95	.0182	.99
14-15	1.90	.0273	1.49	.0189	1.03
15-16	1.20	.0173	.95	.0188	1.02
16-17	1.90	.0274	1.50	.0193	1.05
17-18	1.80	.0259	1.42	.0197	1.07
18-19	3.5	.0504	2.76	.0213	1.16
19-20	4.2	.0605	3.32	.0236	1.28
20-21	1.7	.0244	1.34	.0236	1.28
21-22	.9	.0130	.71	.0231	1.26
22-23	4.5	.0647	3.54	.0250	1.36
23-24	.5	.0072	.39	.0242	1.32
24-25	13.2	.0240	1.31	.0250	1.36
25-26	19.6	.0178	.97	.0218	1.19
26-27	22.0	.0200	1.09	.0214	1.16
27-28	33.5	.0202	1.10	.0210	1.15
28-29	40.0	.0181	.99	.0200	1.09
29-30	36.2	.0164	.90	.0193	1.05
30-31	50.0	.0181	.99	.0190	1.04

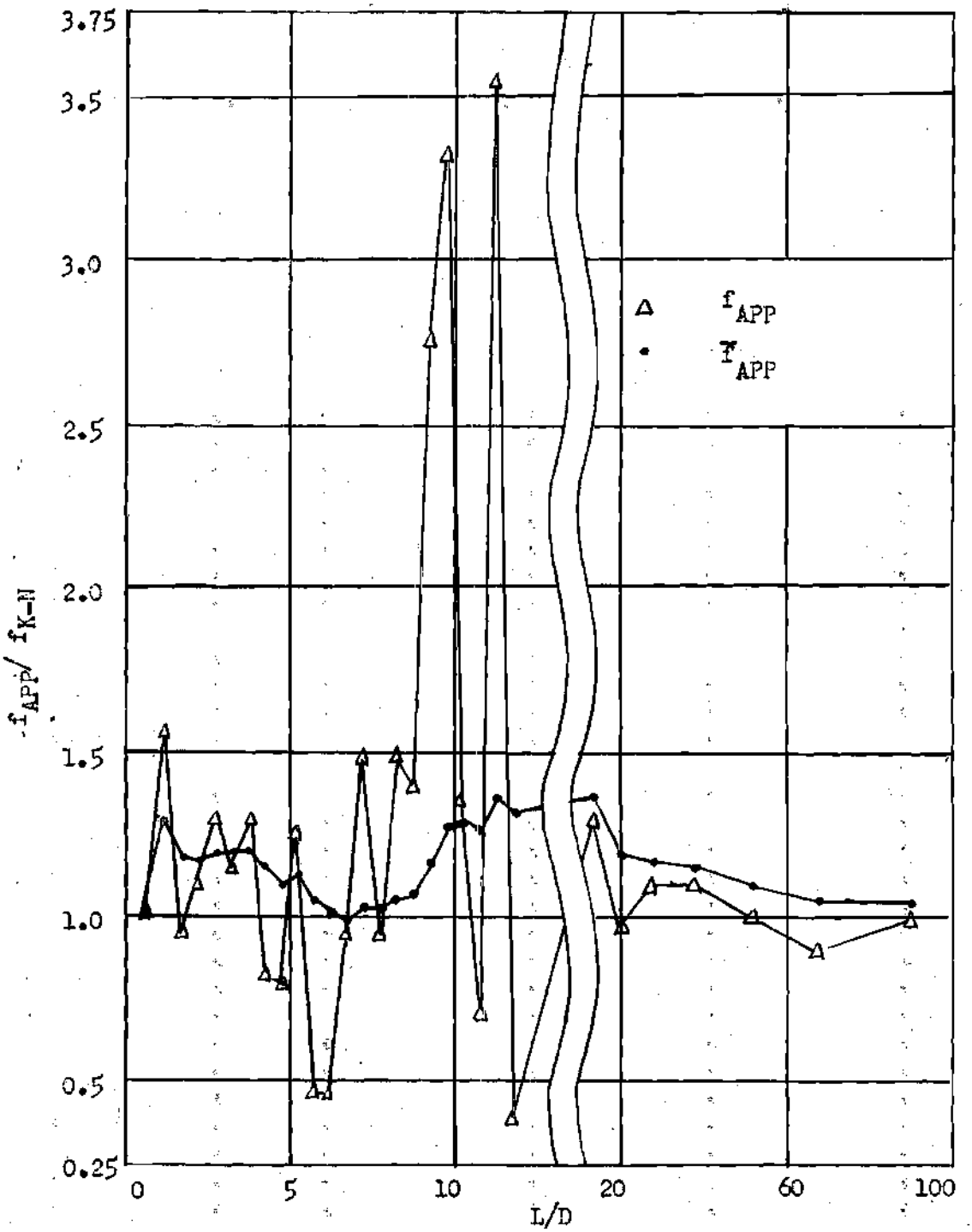

Figure 5. Results for Test E, Entry I. Ratios of local and integrated apparent friction coefficients to the Karman-Nikuradse friction coefficient against L/D for a constant value of R_D.

Table 6. Test F, Entry I

P_{cc} 38 psig

W_w 220 lbs/min.

T_w 53°

R_D 123,000

f_{K-N} .0172

Pressure Taps	ΔP ("H_2O)	f_{APP}	f_{APP}/f_{K-N}	$\overline{f}_{APP}$	$\overline{f}_{APP}/f_{K-N}$
1-2	2.5	.0197	1.15	.0197	1.15
2-3	3.4	.0269	1.56	.0232	1.35
3-4	1.5	.0118	.69	.0193	1.12
4-5	1.3	.0102	.59	.0171	.99
5-6	2.6	.0206	1.20	.0178	1.04
6-7	3.0	.0237	1.38	.0188	1.09
7-8	2.0	.0158	.92	.0183	1.06
8-9	1.7	.0134	.78	.0177	1.03
9-10	3.0	.0237	1.38	.0183	1.06
10-11	4.0	.0316	1.84	.0197	1.15
11-12	4.9	.0387	2.24	.0214	1.25
12-13	2.0	.0158	.92	.0209	1.22
13-14	3.7	.0292	1.70	.0216	1.26
14-15	2.3	.0181	1.05	.0213	1.24
15-16	3.3	.0261	1.52	.0216	1.26
16-17	1.9	.0150	.88	.0212	1.24
17-18	1.6	.0126	.75	.0206	1.20
18-19	2.7	.0214	1.24	.0208	1.21
19-20	1.3	.0103	.60	.0202	1.17
20-21	2.7	.0214	1.24	.0204	1.18
21-22	1.6	.0126	.73	.0198	1.15
22-23	1.7	.0134	.78	.0196	1.14
23-24	1.9	.0150	.87	.0195	1.14
24-25	20.2	.0199	1.16	.0195	1.14
25-26	32.1	.0158	.92	.0183	1.06
26-27	37.2	.0183	1.06	.0183	1.06
27-28	60.5	.0199	1.16	.0182	1.09
28-29	65.0	.0161	.94	.0180	1.05
29-30	68.7	.0170	.99	.0178	1.04
30-31	87.9	.0173	1.01	.0177	1.03

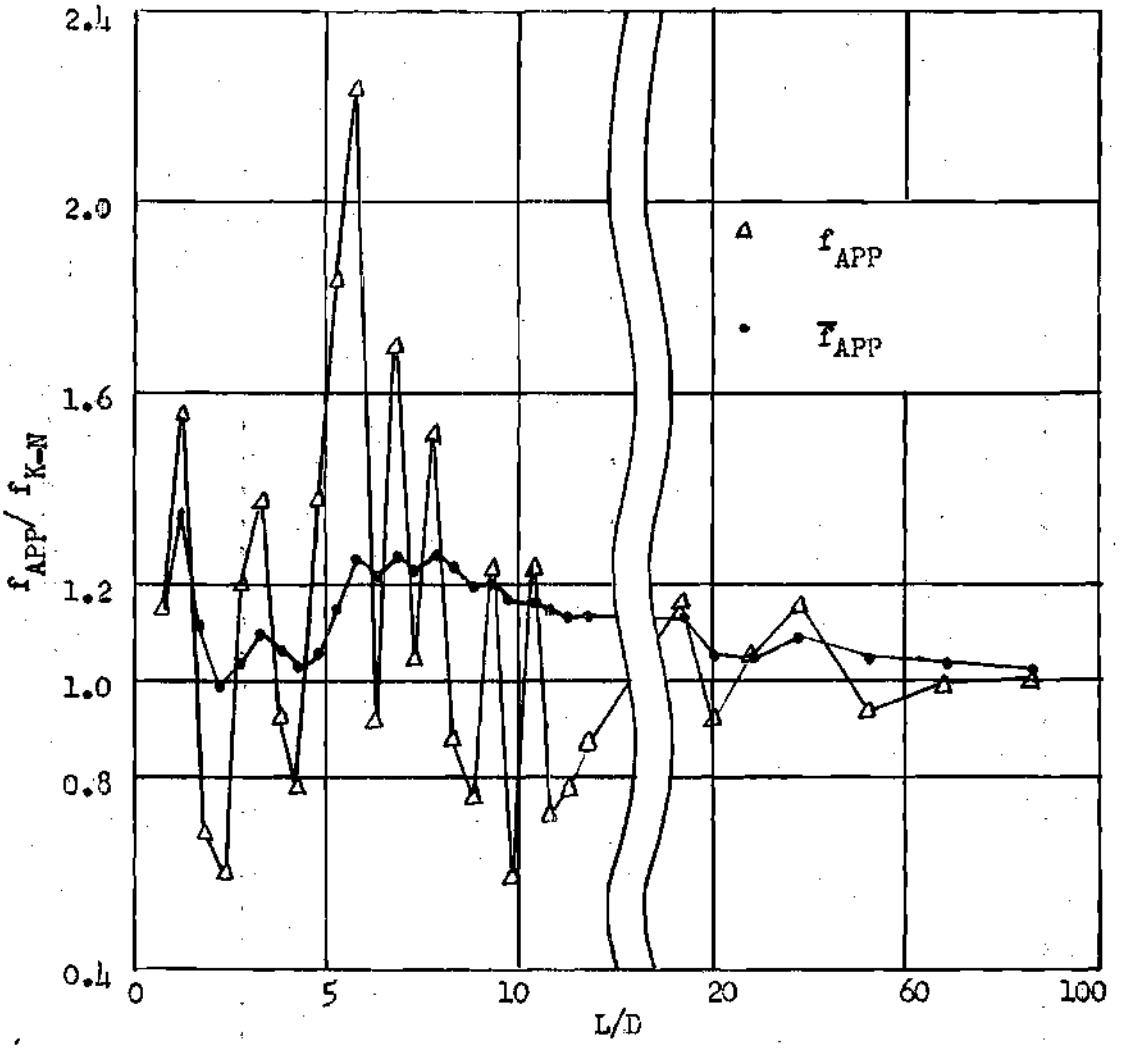

Figure 6. Results for Test F, Entry I. Ratios of local and integrated apparent friction coefficients to the Karman-Nikuradse friction coefficient against L/D for a constant value of R_D.

Table 7. Test G, Entry I

P_{cc}	53 psig	R_D	147,000
W_w	262 lbs/min.	f_{K-N}	.0166
T_w	53°		

Pressure Taps	ΔP ($"H_2O$)	f_{APP}	f_{APP}/f_{K-N}	$\bar{f}_{APP}$	$\bar{f}_{APP}/f_{K-N}$
1-2	3.7	.0180	1.08	.0180	1.08
2-3	4.9	.0238	1.43	.0209	1.26
3-4	1.9	.0093	.56	.0171	1.03
4-5	3.1	.0151	.91	.0165	.99
5-6	4.5	.0219	1.32	.0175	1.05
6-7	4.5	.0219	1.32	.0183	1.10
7-8	4.4	.0214	1.29	.0188	1.13
8-9	6.3	.0307	1.85	.0203	1.22
9-10	5.0	.0244	1.47	.0207	1.24
10-11	3.2	.0156	.94	.0202	1.21
11-12	3.5	.0171	1.03	.0199	1.20
12-13	5.3	.0258	1.56	.0202	1.21
13-14	3.3	.0161	.97	.0200	1.20
14-15	3.2	.0156	.94	.0198	1.19
15-16	4.9	.0238	1.44	.0200	1.20
16-17	6.8	.0331	1.99	.0208	1.25
17-18	1.1	.0054	.33	.0198	1.19
18-19	1.3	.0063	.38	.0192	1.16
19-20	1.2	.0058	.35	.0185	1.11
20-21	5.1	.0248	1.49	.0188	1.13
21-22	5.7	.0278	1.68	.0192	1.16
22-23	4.1	.0200	1.21	.0192	1.16
23-24	4.3	.0210	1.27	.0192	1.16
24-25	29.6	.0180	1.08	.0190	1.14
25-26	41.6	.0127	.76	.0168	1.01
26-27	48.3	.0147	.89	.0163	.98
27-28	101.0	.0205	1.24	.0174	1.05
28-29	111.0	.0170	1.02	.0173	1.04
29-30	113.4	.0173	1.04	.0173	1.04
30-31	128.6	.0157	.95	.0169	1.02

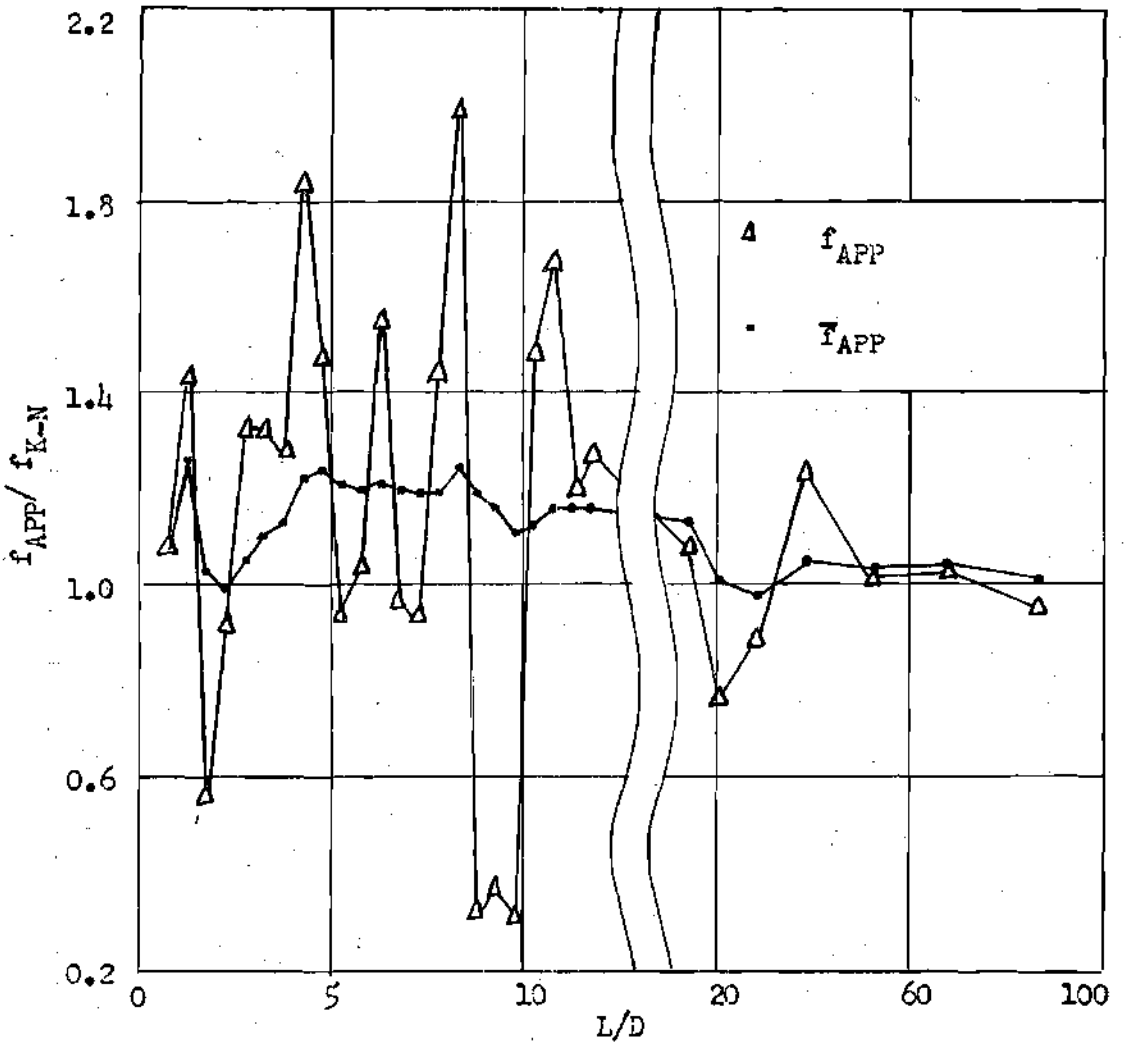

Figure 7. Results for Test G, Entry I. Ratios of local and integrated apparent friction coefficients to the Karman-Nikuradse friction coefficient against L/D for a constant value of R_D.

Table 8. Test A, Entry II

P_{cc} 13.5 psig

W_w 35 lbs/min.

T_w 84°

R_D 29,400

f_{K-N} .0236

Pressure Taps	ΔP ($^{m}H_2O$)	f_{APP}	f_{APP}/f_{K-N}	$\bar{f}_{APP}$	$\bar{f}_{APP}/f_{K-N}$
0-1	.3	.0960	4.08	.0960	4.08
1-2	0			.0481	2.04
2-3	.9	.288	12.2	.129	5.45
3-4	+ .15			.0847	3.59
4-5	+ .65			.0257	1.14
5-6	.12	.0384	1.63	.0276	1.17
6-7	.08	.0256	1.09	.0274	1.16
7-8	.10	.0320	1.36	.0278	1.18
8-9	.11	.0352	1.49	.0286	1.22
9-10	0			.0257	1.14
10-11	.09	.0288	1.22	.0262	1.11
11-12	.07	.0224	.95	.0257	1.14
12-13	.05	.0160	.68	.0276	1.17
13-14	.18	.0575	2.44	.0274	1.16
14-15	.09	.0288	1.23	.0274	1.16
15-16	.08	.0256	1.09	.0272	1.15
16-17	.10	.0320	1.36	.0276	1.16
17-18	.09	.0288	1.23	.0276	1.16
18-19	.04	.0128	.54	.0270	1.14
19-20	.13	.0416	1.77	.0276	1.17
20-21	.10	.0320	1.36	.0278	1.18
21-22	.07	.0224	.95	.0276	1.17
22-23	.06	.0193	.82	.0272	1.15
23-24	.02	.0064	.27	.0264	1.12
24-25	.62	.0248	1.05	.0260	1.10
25-26	1.2	.0248	1.05	.0260	1.10
26-27	1.3	.0260	1.10	.0254	1.08
27-28	2.0	.0267	1.13	.0257	1.09
28-29	2.5	.0250	1.06	.0254	1.08
29-30	2.6	.0260	1.10	.0254	1.08
30-31	3.1	.0248	1.05	.0254	1.08

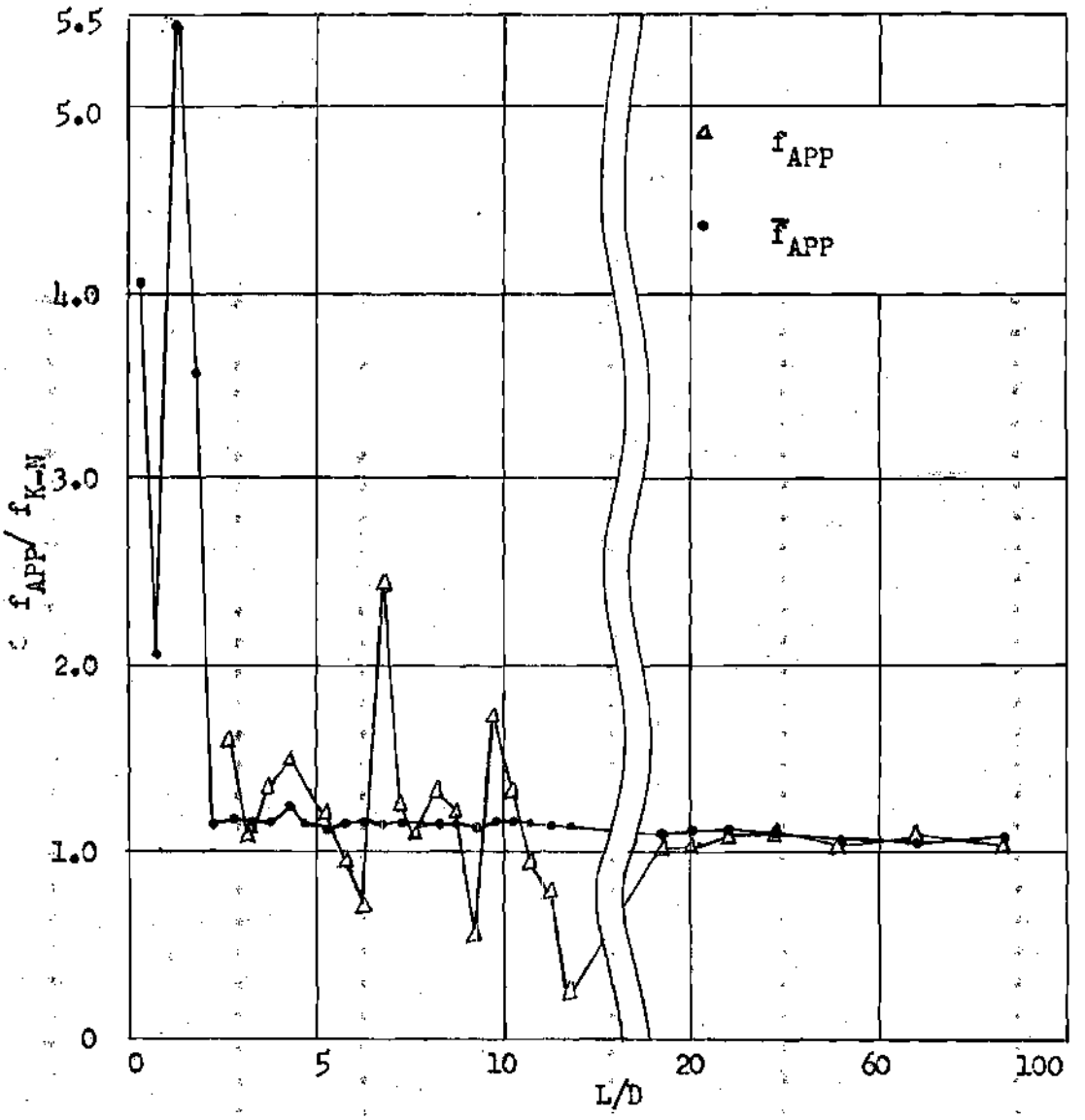

Figure 8. Results for Test A, Entry II. Ratios of local and integrated apparent friction coefficients to the Karman-Nikuradse friction coefficient against L/D for a constant value of R_D.

Table 9. Test B, Entry II

P_{cc} 18.5 psig

W_w 59.5 lbs/min.

T_w 84°

R_D 50,500

f_{K-N} .0209

Pressure Taps	ΔP ($"H_2O$)	f_{APP}	f_{APP}/f_{K-N}	$\bar{f}_{APP}$	$\bar{f}_{APP}/f_{K-N}$
0-1	.8	.0878	4.20	.0878	4.20
1-2	.1	.0196	.94	.0494	2.36
2-3	1.35	.148	7.08	.0820	3.92
3-4	+ .37			.0515	2.46
4-5	+ .78			.0238	1.14
5-6	.19	.0208	1.0	.0236	1.13
6-7	.19	.0208	1.0	.0232	1.11
7-8	.27	.0296	1.42	.0240	1.15
8-9	.29	.0318	1.52	.0247	1.18
9-10	.12	.0132	.63	.0236	1.13
10-11	.15	.0164	.79	.0230	1.10
11-12	.27	.0296	1.42	.0234	1.12
12-13	.22	.0242	1.16	.0239	1.15
13-14	.22	.0242	1.16	.0236	1.13
14-15	.16	.0176	.84	.0232	1.11
15-16	.18	.0198	.95	.0230	1.10
16-17	.22	.0242	1.16	.0230	1.10
17-18	.16	.0176	.84	.0228	1.09
18-19	.31	.0340	1.63	.0234	1.12
19-20	.36	.0395	1.89	.0242	1.16
20-21	.30	.0329	1.58	.0246	1.18
21-22	.14	.0154	.74	.0242	1.16
22-23	.18	.0198	.95	.0240	1.15
23-24	.17	.0187	.90	.0236	1.13
24-25	1.60	.0219	1.05	.0234	1.12
25-26	3.4	.0233	1.12	.0234	1.12
26-27	3.3	.0226	1.08	.0232	1.11
27-28	5.1	.0233	1.12	.0232	1.11
28-29	6.6	.0226	1.08	.0230	1.10
29-30	6.0	.0206	.99	.0226	1.08
30-31	8.0	.0219	1.05	.0224	1.07

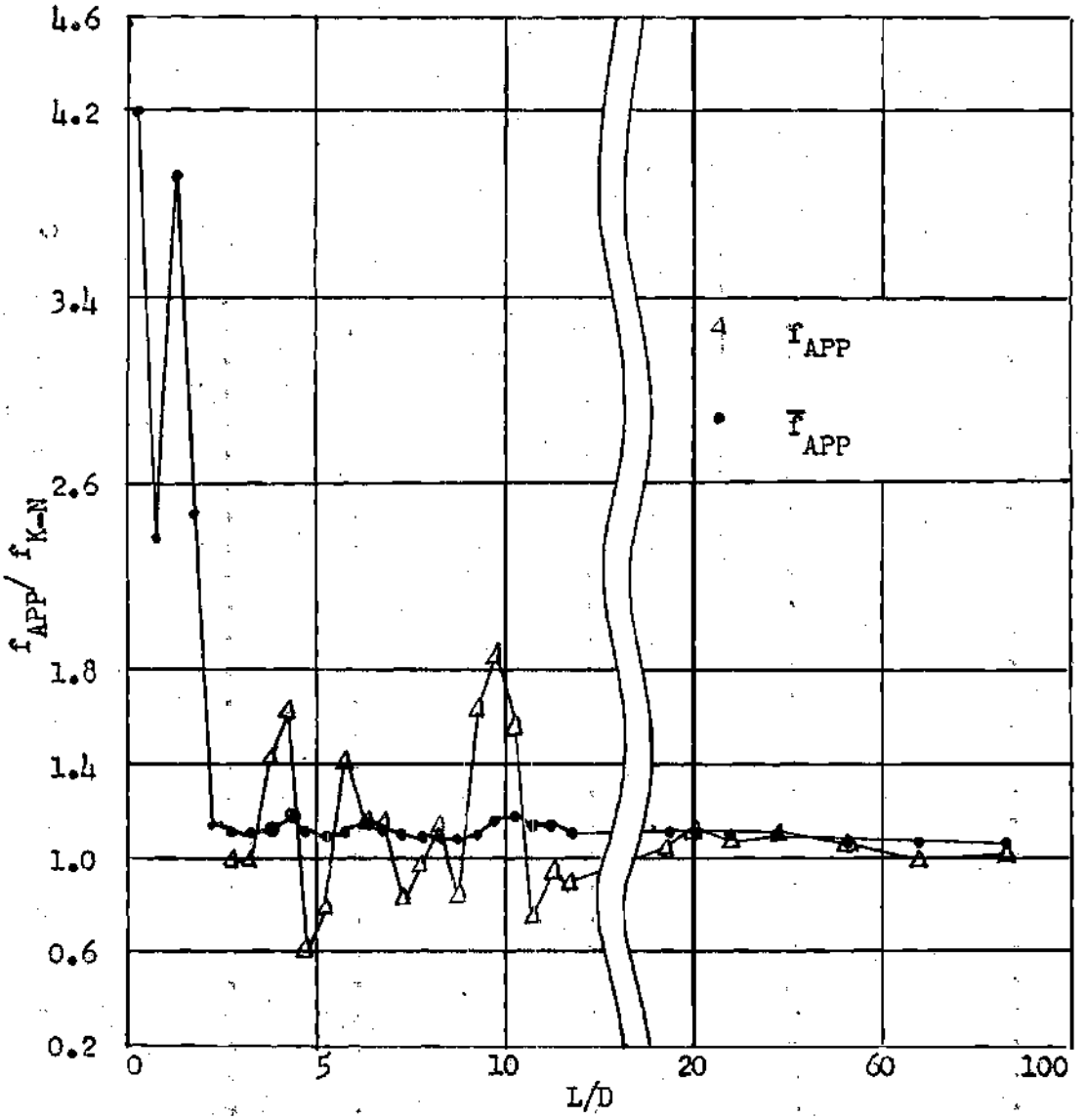

Figure 9. Results for Test B, Entry II. Ratios of local and integrated apparent friction coefficients to the Karman-Nikuradse friction coefficient against L/D for a constant value of R_D.

Table 10. Test C, Entry II

P_{cc}	23 psig	R_D	69,000
W_w	81 lbs/min.	f_{K-N}	.0195
T_w	84°		

Pressure Taps	ΔP ($"H_2O$)	f_{APP}	f_{APP}/f_{K-N}	$\bar{f}_{APP}$	$\bar{f}_{APP}/f_{K-N}$
0-1	.90	.0525	2.70	.0525	2.70
1-2	.30	.0177	.91	.0349	1.79
2-3	2.70	.1590	8.17	.0767	3.93
3-4	+ .36			.0520	2.67
4-5	+1.65			.0220	1.14
5-6	.35	.0206	1.06	.0220	1.13
6-7	.36	.0212	1.09	.0218	1.12
7-8	.45	.0265	1.36	.0224	1.15
8-9	.45	.0265	1.36	.0230	1.18
9-10	.28	.0165	.85	.0222	1.14
10-11	.18	.0106	.55	.0212	1.09
11-12	.36	.0212	1.09	.0212	1.09
12-13	.41	.0242	1.24	.0214	1.10
13-14	.42	.0247	1.27	.0216	1.11
14-15	.35	.0206	1.06	.0216	1.11
15-16	.50	.0294	1.51	.0220	1.13
16-17	.30	.0177	.91	.0218	1.12
17-18	.30	.0177	.91	.0216	1.11
18-19	.5	.0294	1.51	.0220	1.13
19-20	.45	.0265	1.36	.0222	1.14
20-21	.75	.0442	2.27	.0232	1.19
21-22	.25	.0147	.76	.0228	1.17
22-23	.25	.0147	.76	.0224	1.15
23-24	.25	.0147	.76	.0222	1.14
24-25	2.95	.0218	1.12	.0220	1.13
25-26	5.8	.0213	1.09	.0218	1.12
26-27	5.4	.0198	1.02	.0214	1.10
27-28	8.5	.0208	1.07	.0212	1.09
28-29	12.4	.0228	1.17	.0216	1.11
29-30	10.2	.0188	.97	.0210	1.08
30-31	15.0	.0220	1.13	.0212	1.09

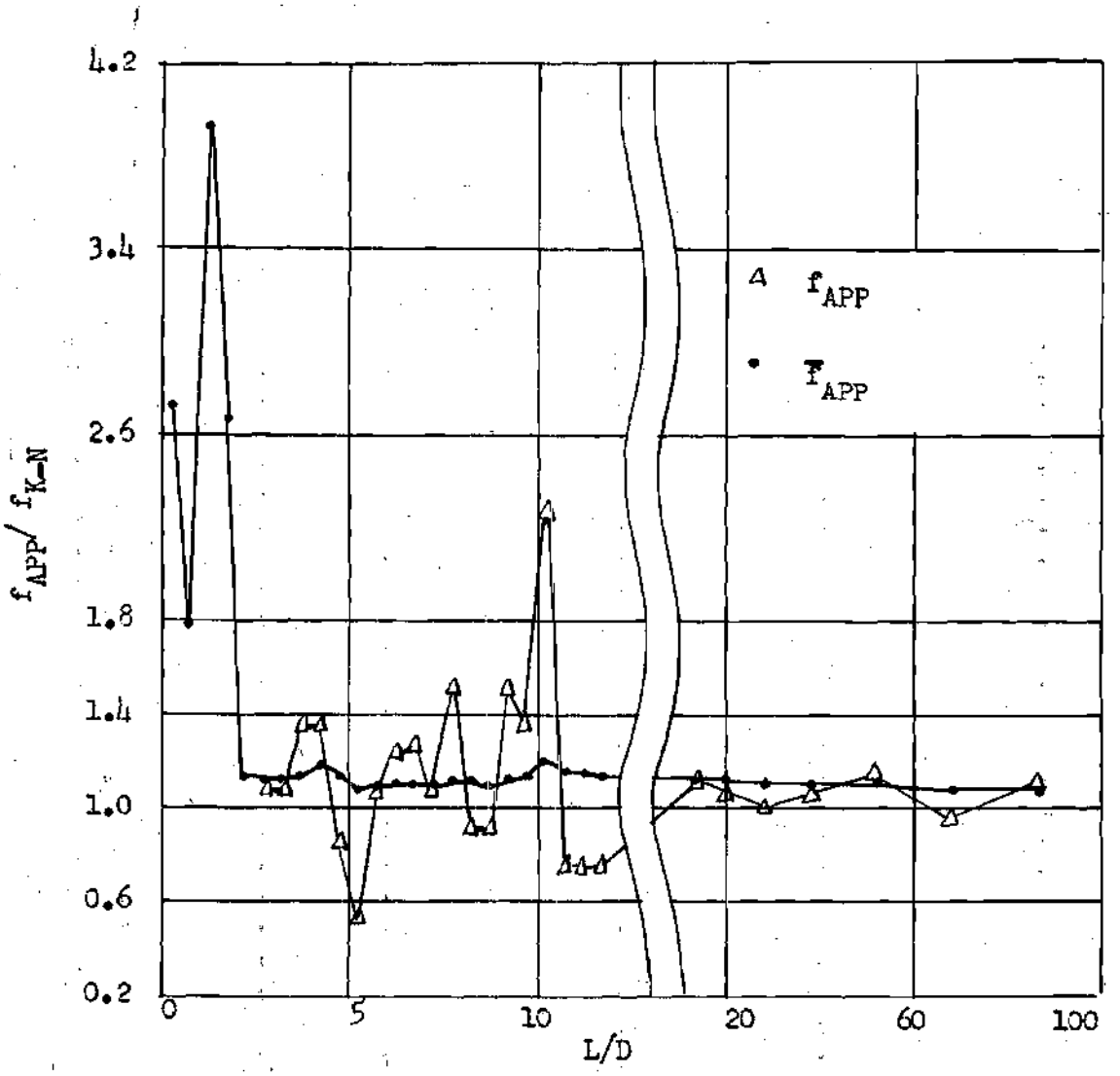

Figure 10. Results for Test C, Entry II. Ratios of local and integrated apparent friction coefficients to the Karman-Nikuradse friction coefficient against L/D for a constant value of R_D.

Table 11. Test D, Entry II

P_{cc} 22 psig

W_w 97 lbs/min.

T_w 83½°

R_D 81,300

f_{K-N} .0188

Pressure Taps	ΔP ("H_2O)	f_{APP}	f_{APP}/f_{K-N}	$\bar{f}_{APP}$	$\bar{f}_{APP}/f_{K-N}$
0-1	1.3	.0543	2.89	.0543	2.88
1-2	1.2	.0502	2.68	.0522	2.78
2-3	2.2	.0902	4.80	.0654	3.48
3-4	+ .4			.0447	2.38
4-5	+ 1.6			.0226	1.20
5-6	.5	.0209	1.11	.0224	1.19
6-7	.5	.0209	1.11	.0220	1.17
7-8	.5	.0209	1.11	.0220	1.17
8-9	.5	.0209	1.11	.0218	1.16
9-10	.4	.0167	.89	.0214	1.14
10-11	.35	.0146	.78	.0208	1.11
11-12	.6	.0250	1.32	.0211	1.13
12-13	.5	.0209	1.11	.0211	1.13
13-14	.4	.0167	.89	.0208	1.11
14-15	.5	.0209	1.11	.0208	1.11
15-16	.6	.0250	1.32	.0210	1.12
16-17	.15	.0063	.34	.0202	1.07
17-18	.5	.0209	1.11	.0202	1.07
18-19	.8	.0334	1.78	.0209	1.11
19-20	.5	.0209	1.11	.0210	1.12
20-21	1.05	.0439	2.34	.0220	1.17
21-22	.35	.0146	.78	.0216	1.15
22-23	.4	.0167	.89	.0214	1.14
23-24	.25	.0105	.56	.0210	1.12
24-25	3.8	.0198	1.05	.0207	1.10
25-26	7.95	.0208	1.11	.0207	1.10
26-27	8.05	.0211	1.12	.0207	1.10
27-28	10.95	.0191	1.02	.0203	1.08
28-29	16.1	.0210	1.12	.0205	1.09
29-30	15.4	.0201	1.07	.0204	1.08
30-31	18.9	.0198	1.05	.0203	1.08

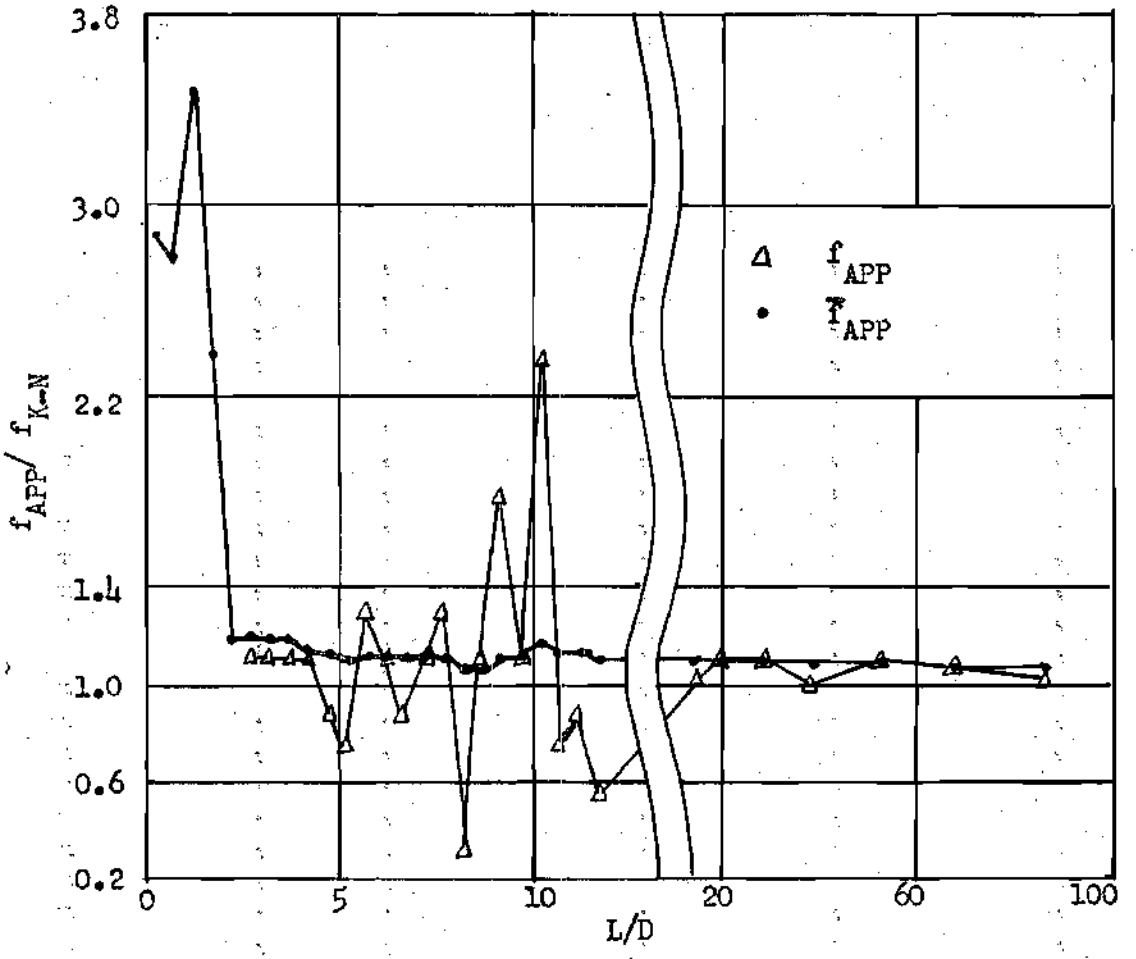

Figure 11. Results for Test D, Entry II. Ratios of local and integrated apparent friction coefficients to the Karman-Nikuradse friction coefficient against L/D for a constant value of R_D.

Table 12. Test E, Entry II

P_{cc}	18 psig	R_D	88,400
W_w	105 lbs/min.	f_{K-N}	.0185
T_w	85°		

Pressure Taps	ΔP ($"H_2O$)	f_{APP}	f_{APP}/f_{K-N}	$\bar{f}_{APP}$	$\bar{f}_{APP}/f_{K-N}$
0-1	.9	.0323	1.75	.0323	1.75
1-2	1.9	.0680	3.68	.0503	2.72
2-3	2.45	.0878	4.75	.0630	3.40
3-4	+ .75			.0405	2.19
4-5	+ 1.3			.0230	1.24
5-6	.7	.0251	1.36	.0233	1.26
6-7	.65	.0233	1.26	.0232	1.25
7-8	.6	.0215	1.16	.0230	1.24
8-9	.4	.0143	.77	.0220	1.19
9-10	.4	.0143	.77	.0214	1.16
10-11	.4	.0143	.77	.0206	1.11
11-12	.6	.0215	1.16	.0208	1.12
12-13	.55	.0197	1.06	.0206	1.11
13-14	.65	.0233	1.26	.0208	1.12
14-15	.6	.0215	1.16	.0209	1.13
15-16	.7	.0251	1.36	.0211	1.14
16-17	.45	.0162	.88	.0208	1.12
17-18	.15	.0054	.29	.0200	1.08
18-19	.35	.0125	.68	.0196	1.06
19-20	1.0	.0358	1.94	.0204	1.10
20-21	.4	.0143	.77	.0201	1.09
21-22	1.0	.0358	1.94	.0208	1.12
22-23	.4	.0143	.77	.0206	1.11
23-24	.2	.0072	.39	.0200	1.08
24-25	4.5	.0202	1.09	.0200	1.08
25-26	8.9	.0199	1.08	.0200	1.08
26-27	9.3	.0209	1.13	.0202	1.09
27-28	12.8	.0191	1.03	.0199	1.08
28-29	17.0	.0190	1.03	.0197	1.07
29-30	17.4	.0195	1.05	.0196	1.06
30-31	21.3	.0191	1.03	.0195	1.05

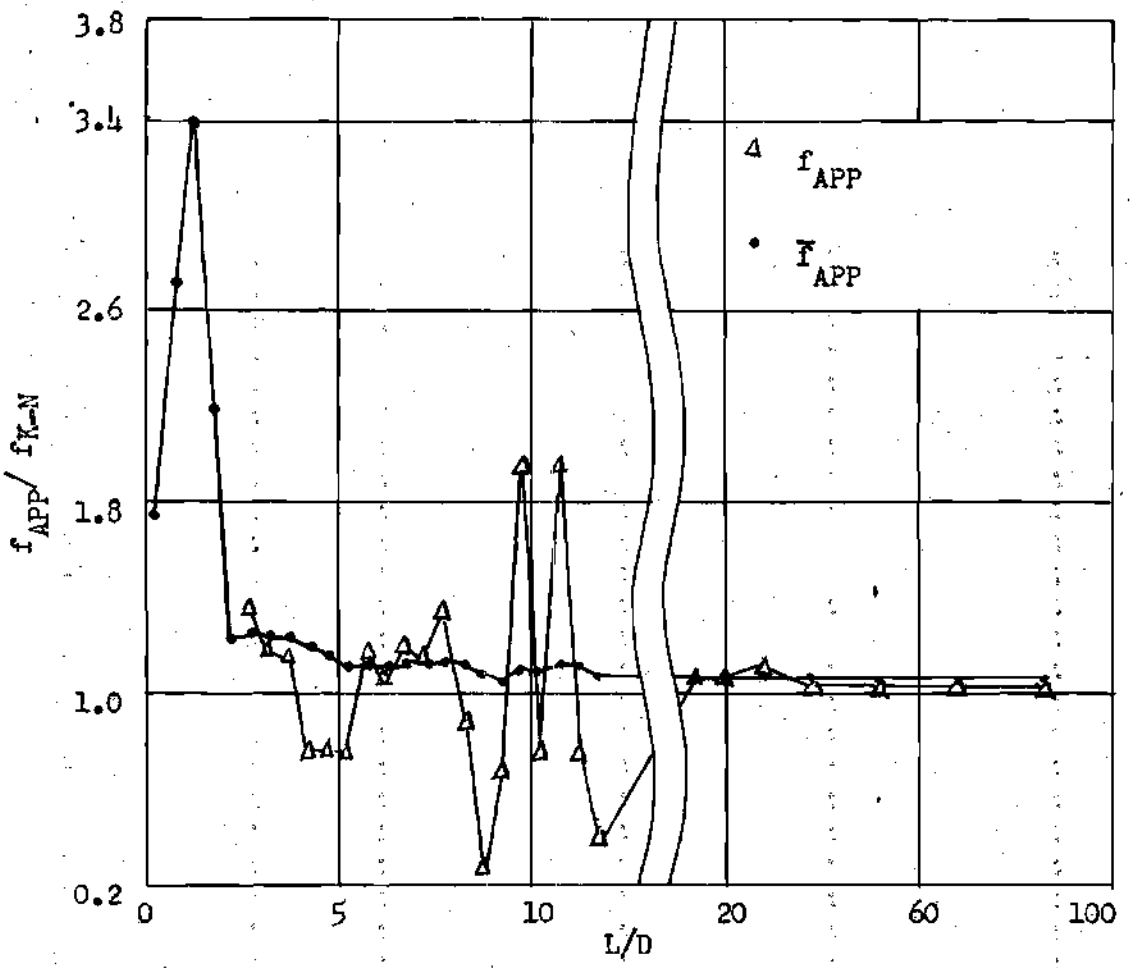

Figure 12. Results for Test E, Entry II. Ratios of local and integrated apparent friction coefficients to the Karman-Nikuradse friction coefficients against L/D for a constant value of R_D.

Table 13. Test F, Entry II

P_{cc}	20 psig	R_D	116,000
W_w	138 lbs/min.	f_{K-N}	.0174
T_w	84°		

Pressure Taps	ΔP ($"H_2O$)	f_{APP}	f_{APP}/f_{K-N}	$\bar{f}_{APP}$	$\bar{f}_{APP}/f_{K-N}$
0-1	1.1	.0227	1.31	.0227	1.31
1-2	3.3	.0680	3.92	.0452	2.60
2-3	3.95	.0815	4.69	.0572	3.29
3-4	+ 1.05			.0376	2.16
4-5	+ 1.2			.0251	1.44
5-6	.7	.0144	.83	.0234	1.34
6-7	.75	.0155	.89	.0223	1.28
7-8	1.05	.0216	1.24	.0222	1.27
8-9	1.3	.0268	1.54	.0226	1.30
9-10	.8	.0165	.95	.0220	1.26
10-11	1.4	.0288	1.66	.0228	1.31
11-12	.25	.0052	.30	.0212	1.22
12-13	.25	.0052	.30	.0200	1.15
13-14	1.0	.0206	1.19	.0200	1.15
14-15	.9	.0186	1.07	.0199	1.14
15-16	.9	.0186	1.07	.0198	1.14
16-17	.7	.0144	.83	.0195	1.12
17-18	1.4	.0288	1.66	.0200	1.15
18-19	1.3	.0268	1.54	.0204	1.17
19-20	1.6	.0330	1.90	.0211	1.21
20-21	1.4	.0288	1.66	.0214	1.23
21-22	.5	.0103	.59	.0209	1.20
22-23	.7	.0144	.83	.0206	1.18
23-24	.7	.0144	.83	.0204	1.17
24-25	7.1	.0183	1.05	.0198	1.14
25-26	14.2	.0183	1.05	.0193	1.11
26-27	15.0	.0192	1.10	.0193	1.11
27-28	21.0	.0189	1.09	.0192	1.10
28-29	28.5	.0183	1.05	.0190	1.09
29-30	28.0	.0180	1.04	.0188	1.08
30-31	34.4	.0177	1.02	.0186	1.07

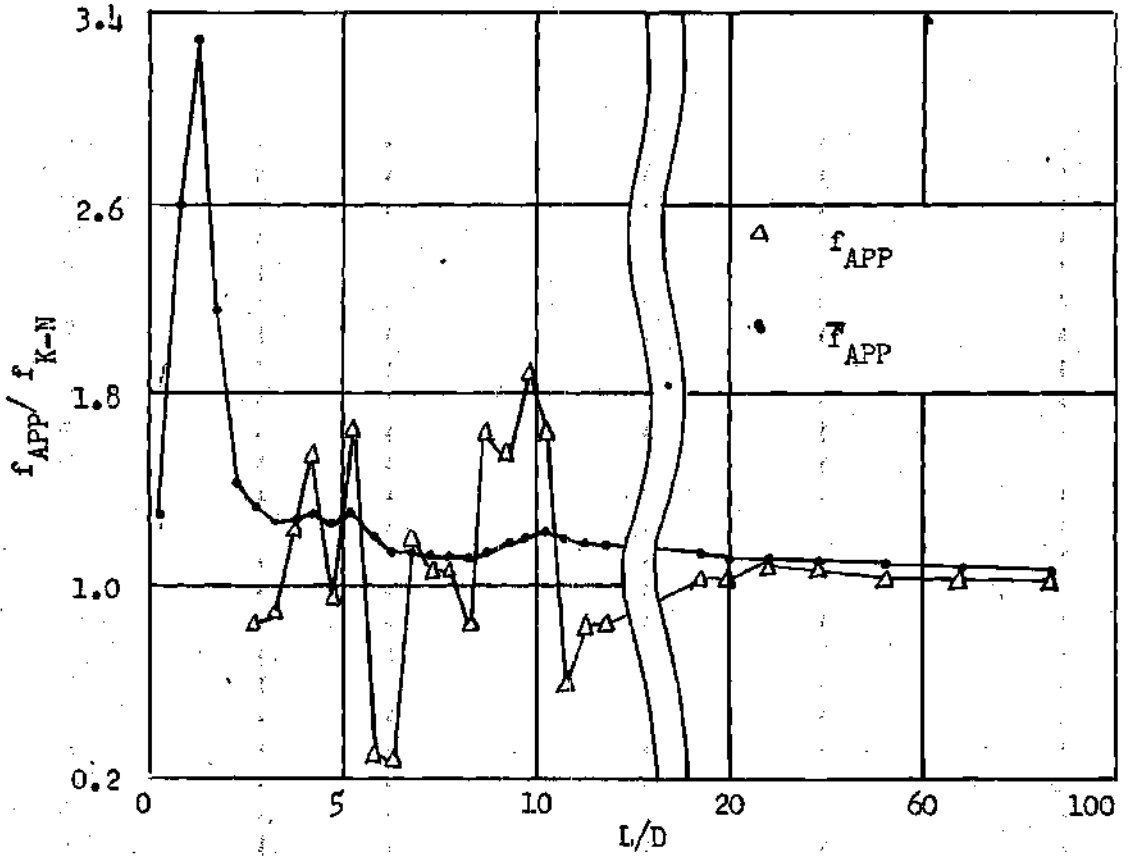

Figure 13. Results for Test F, Entry II. Ratios of local and integrated apparent friction coefficients to the Karman-Nikuradse friction coefficient against L/D for a constant value of R_D.

Table 14. Test G, Entry II

P_{cc} 24 psig

W_w 177 lbs/min.

T_w 84°

R_D 149,500

f_{K-N} .0166

Pressure Taps	ΔP ($"H_2O$)	f_{APP}	f_{APP}/f_{K-N}	$\bar{f}_{APP}$	$\bar{f}_{APP}/f_{K-N}$
0-1	1.6	.0199	1.20	.0199	1.20
1-2	5.05	.0630	3.78	.0415	2.50
2-3	5.85	.0730	4.38	.0521	3.14
3-4	0			.0390	2.35
4-5	+ .6			.0298	1.80
5-6	1.0	.0125	.75	.0268	1.61
6-7	1.0	.0125	.75	.0248	1.49
7-8	1.6	.0199	1.20	.0242	1.46
8-9	1.5	.0187	1.12	.0236	1.42
9-10	1.3	.0162	.97	.0228	1.37
10-11	1.2	.0149	.90	.0222	1.34
11-12	.5	.0062	.37	.0209	1.26
12-13	.3	.0038	.23	.0195	1.18
13-14	.5	.0062	.37	.0186	1.12
14-15	.4	.0049	.29	.0177	1.07
15-16	2.1	.0262	1.57	.0182	1.10
16-17	.9	.0112	.67	.0178	1.07
17-18	2.0	.0250	1.50	.0182	1.10
18-19	2.5	.0312	1.87	.0189	1.14
19-20	2.2	.0274	1.65	.0193	1.16
20-21	1.1	.0137	.82	.0191	1.15
21-22	1.0	.0125	.75	.0188	1.13
22-23	1.2	.0149	.90	.0186	1.12
23-24	.6	.0075	.45	.0181	1.09
24-25	10.4	.0162	.97	.0177	1.07
25-26	22.8	.0178	1.07	.0177	1.07
26-27	22.0	.0171	1.03	.0176	1.06
27-28	34.0	.0177	1.06	.0176	1.06
28-29	43.2	.0169	1.02	.0174	1.05
29-30	44.2	.0172	1.03	.0174	1.05
30-31	55.0	.0171	1.03	.0173	1.04

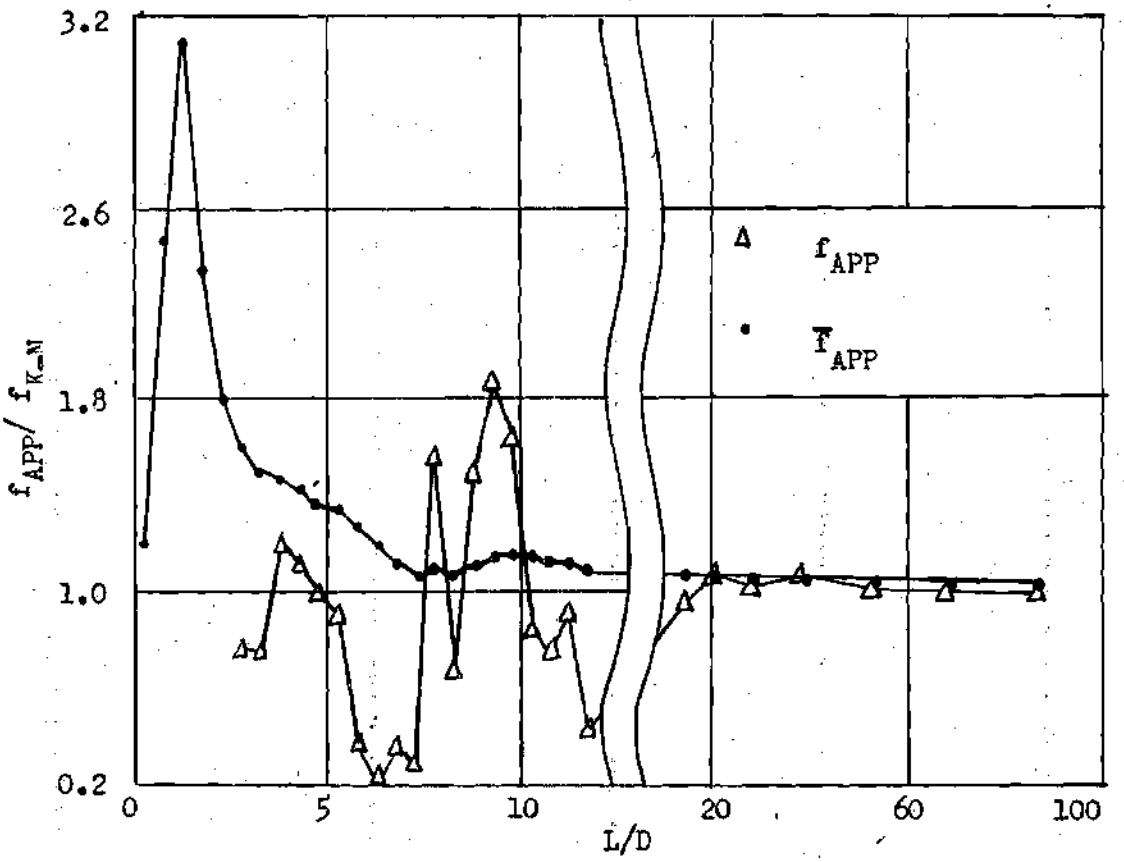

Figure 14. Results for Test G, Entry II. Ratios of local and integrated apparent friction coefficients to the Karman-Nikuradse friction coefficient against L/D for a constant value of R_D.

Table 15. Test A, Entry III

P_{cc}	20 psig	R_D	30,600
W_w	37 lbs/min.	f_{K-N}	.0234
T_w	83°		

Pressure Taps	ΔP ("H_2O)	f_{APP}	f_{APP}/f_{K-N}	$\bar{f}_{APP}$	$\bar{f}_{APP}/f_{K-N}$
0-1	45.6	13.08	560	13.08	560
1-2	+ 44.805			.1145	4.90
2-3	+ .06			.0705	3.02
3-4	+ .035			.0504	2.16
4-5	+ .02			.0380	1.62
5-6	+ .01			.0320	1.36
6-7	.05	.0143	.61	.0296	1.26
7-8	.035	.0100	.43	.0271	1.16
8-9	.045	.0129	.55	.0256	1.10
9-10	.07	.0200	.86	.0250	1.07
10-11	.105	.0301	1.29	.0255	1.09
11-12	.12	.0344	1.47	.0262	1.12
12-13	.10	.0286	1.22	.0264	1.13
13-14	.095	.0272	1.16	.0266	1.14
14-15	.095	.0272	1.16	.0266	1.14
15-16	.135	.0387	1.65	.0273	1.17
16-17	.04	.0115	.49	.0264	1.13
17-18	.06	.0172	.74	.0256	1.09
18-19	.03	.0086	.37	.0250	1.07
19-20	.075	.0214	.92	.0248	1.06
20-21	.085	.0244	1.04	.0248	1.06
21-22	.09	.0258	1.10	.0248	1.06
22-23	.07	.0200	.86	.0246	1.05
23-24	.10	.0286	1.22	.0248	1.06
24-25	.67	.0240	1.03	.0246	1.05
25-26	1.37	.0246	1.05	.0246	1.05
26-27	1.41	.0252	1.08	.0248	1.06
27-28	1.92	.0230	.99	.0243	1.04
28-29	2.71	.0243	1.04	.0243	1.04
29-30	2.60	.0233	1.0	.0241	1.03
30-31	3.15	.0227	.97	.0238	1.02

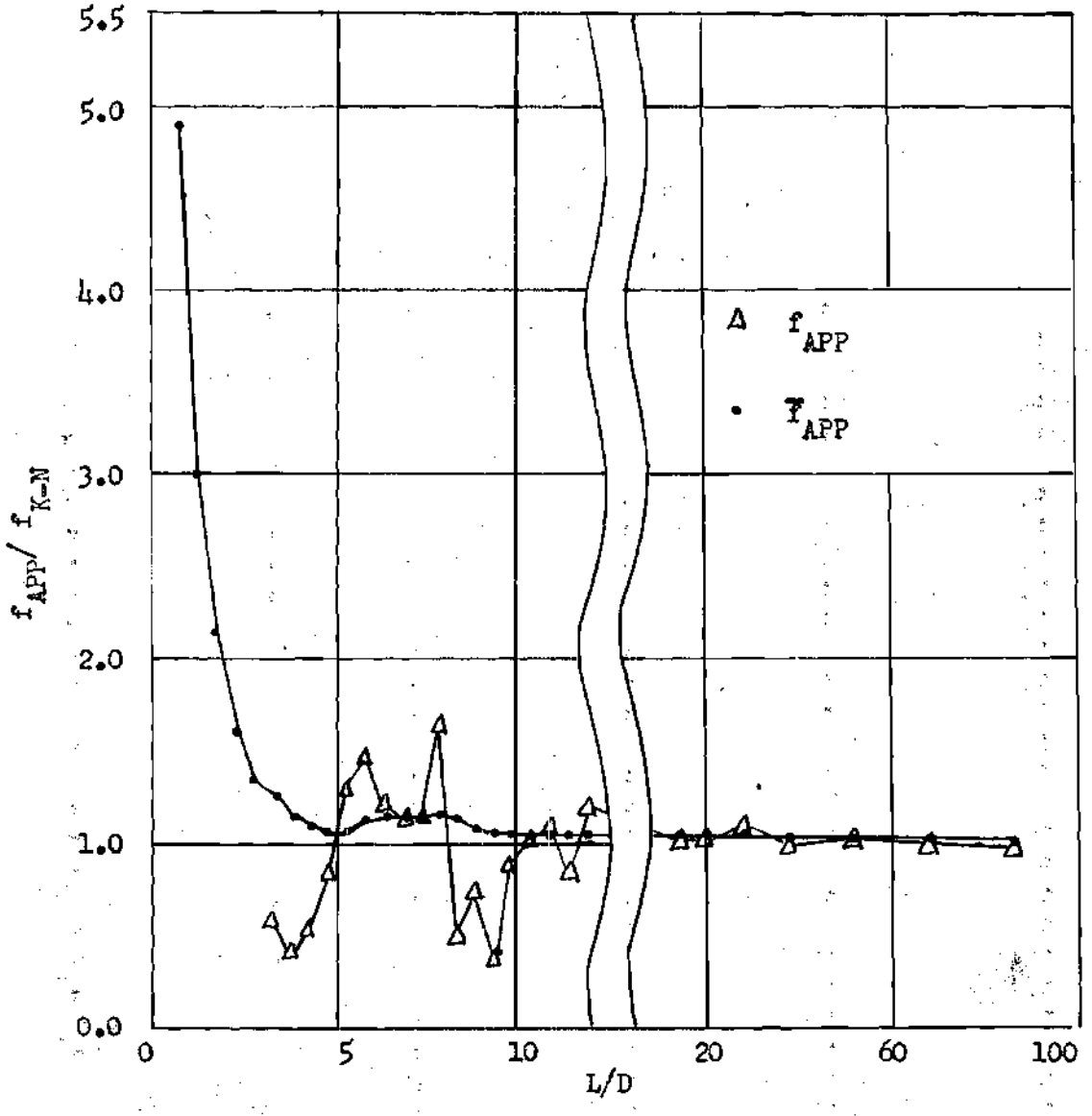

Figure 15. Results for Test A_p, Entry III. Ratios of local and integrated apparent friction coefficients to the Karman-Nikuradse friction coefficient against L/D for a constant value of R_D.

Table 16. Test B, Entry III

P_{cc} 20 psig R_D 50,300

W_w 61 lbs/min. f_{K-N} .0209

T_w 83°

Pressure Taps	ΔP ($"H_2O$)	f_{APP}	f_{APP}/f_{K-N}	$\bar{f}_{APP}$	$\bar{f}_{APP}/f_{K-N}$
0-1	35.3	3.790	182	3.790	182
1-2	+33.38			.1030	4.94
2-3	+ .12			.0643	3.08
3-4	+ .295			.0405	1.94
4-5	+ .105			.0300	1.44
5-6	.095	.0102	.49	.0268	1.29
6-7	.20	.0216	1.04	.0260	1.24
7-8	.185	.0199	.95	.0253	1.21
8-9	.05	.0054	.26	.0230	1.10
9-10	.19	.0204	.98	.0228	1.09
10-11	.195	.0210	1.01	.0226	1.08
11-12	.18	.0194	.93	.0224	1.07
12-13	.26	.0260	1.25	.0228	1.09
13-14	.105	.0103	.49	.0226	1.08
14-15	.335	.0361	1.73	.0229	1.10
15-16	.325	.0350	1.68	.0237	1.13
16-17	.15	.0161	.77	.0232	1.11
17-18	.07	.0075	.36	.0224	1.07
18-19	.29	.0312	1.50	.0228	1.09
19-20	.18	.0194	.93	.0226	1.08
20-21	.285	.0307	1.47	.0230	1.10
21-22	.255	.0275	1.32	.0232	1.11
22-23	.17	.0183	.88	.0230	1.10
23-24	.16	.0172	.83	.0228	1.09
24-25	1.65	.0221	1.06	.0226	1.08
25-26	3.35	.0226	1.08	.0226	1.08
26-27	3.22	.0216	1.04	.0224	1.07
27-28	4.70	.0211	1.01	.0220	1.05
28-29	6.35	.0213	1.02	.0218	1.04
29-30	6.25	.0210	1.01	.0217	1.04
30-31	8.0	.0216	1.04	.0216	1.03

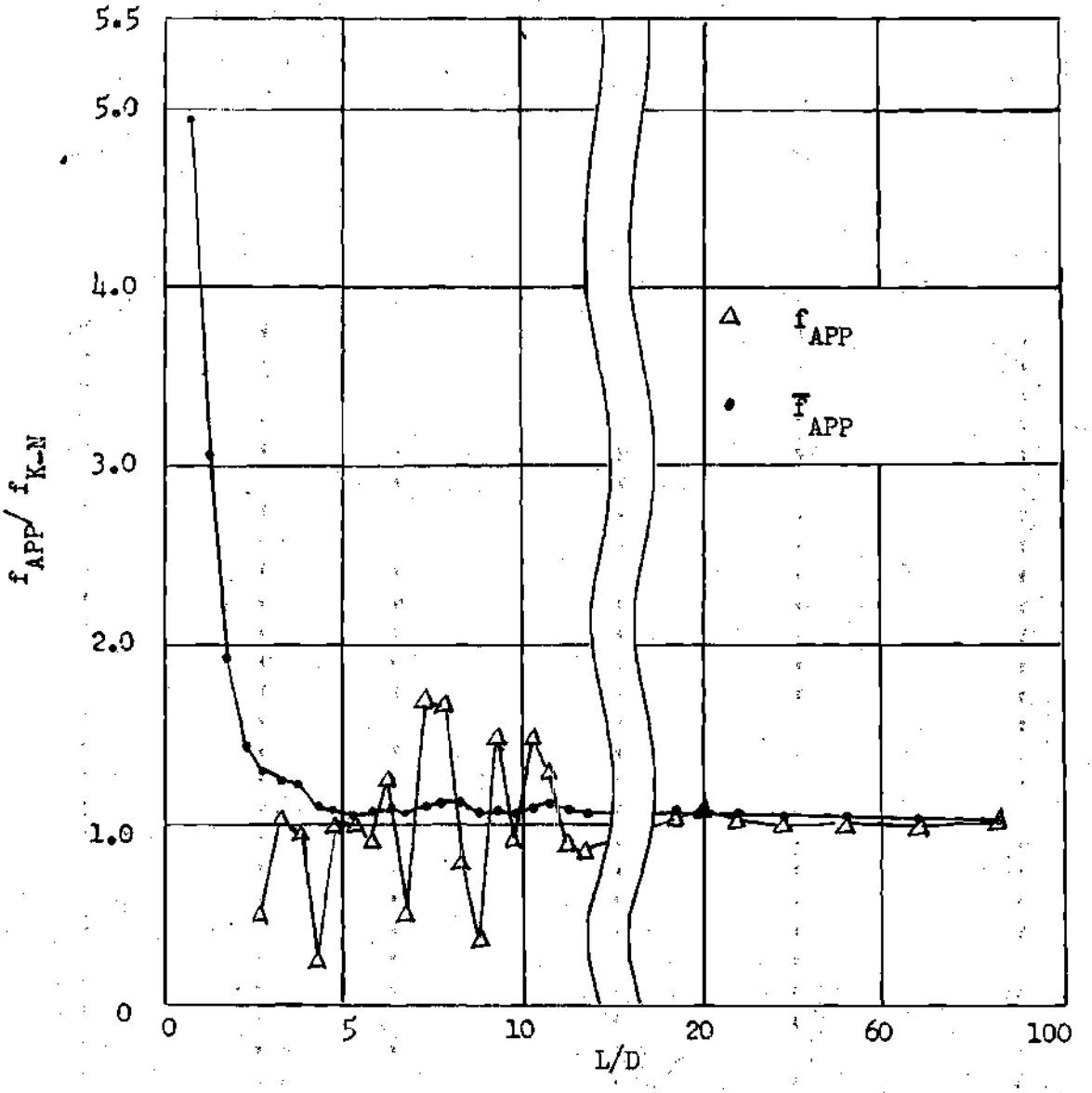

Figure 16. Results for Test B, Entry III. Ratios of local and integrated apparent friction coefficients to the Karman-Nikuradse friction coefficient against L/D for a constant value of R_D.

Table 17. Test C, Entry III

P_{cc}	18 psig	R_D	65,500
W_w	79 lbs/min.	f_{K-N}	.0197
T_w	83°		

Pressure Taps	ΔP ("H_2O)	f_{APP}	f_{APP}/f_{K-N}	$\bar{f}_{APP}$	$\bar{f}_{APP}/f_{K-N}$
0-1	26.8	1.67	84.7	1.67	84.7
1-2	+ 23.68			.0968	4.81
2-3	+ .20			.0605	3.07
3-4	+ .81			.0312	1.58
4-5	.20	.0124	.63	.0274	1.39
5-6	.285	.0177	.90	.0258	1.31
6-7	.145	.0095	.48	.0234	1.19
7-8	.17	.0106	.54	.0218	1.11
8-9	.33	.0206	1.05	.0217	1.10
9-10	.28	.0174	.88	.0213	1.08
10-11	.40	.0249	1.26	.0216	1.09
11-12	.08	.0050	.25	.0202	1.03
12-13	.65	.0404	2.05	.0217	1.10
13-14	.28	.0174	.88	.0214	1.09
14-15	.65	.0404	2.05	.0227	1.15
15-16	.45	.0280	1.42	.0230	1.17
16-17	.12	.0075	.38	.0221	1.12
17-18	.18	.0112	.57	.0215	1.09
18-19	.29	.0181	.92	.0213	1.08
19-20	.44	.0274	1.39	.0216	1.10
20-21	.46	.0286	1.45	.0219	1.11
21-22	.08	.0050	.25	.0212	1.07
22-23	.47	.0292	1.48	.0215	1.09
23-24	.27	.0169	.86	.0213	1.08
24-25	2.64	.0206	1.05	.0211	1.07
25-26	5.27	.0205	1.04	.0209	1.06
26-27	5.05	.0197	1.0	.0205	1.04
27-28	7.9	.0206	1.05	.0205	1.04
28-29	10.4	.0203	1.03	.0204	1.04
29-30	10.1	.0197	1.00	.0203	1.03
30-31	13.1	.0204	1.04	.0203	1.03

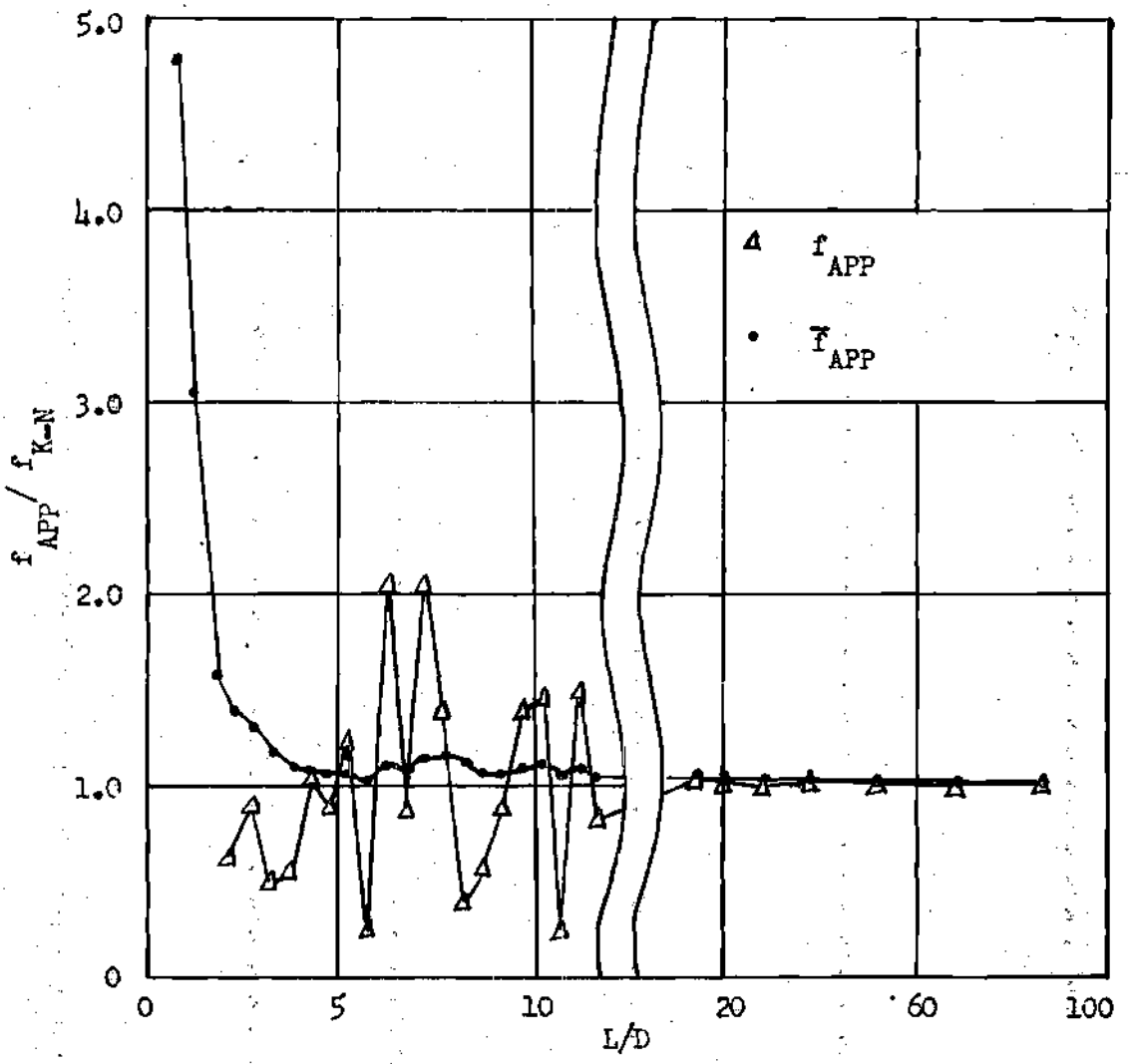

Figure 17. Results for Test C, Entry III. Ratios of local and integrated apparent friction coefficients to the Karman-Nikuradse friction coefficient against L/D for a constant value of R_D.

Table 18. Test D, Entry III

P_{cc} 20 psig

W_w 97½ lbs/min.

T_w 83°

R_D 80,300

f_{K-N} .0188

Pressure Taps	ΔP ("H_2O)	f_{APP}	f_{APP}/f_{K-N}	$\overline{f}_{APP}$	$\overline{f}_{APP}/f_{K-N}$
0-1	28.5	1.18	64.0	1.18	64.0
1-2	+ 24.9			.0745	3.96
2-3	+ .17			.0474	2.52
3-4	+ .73			.0280	2.02
4-5	.70	.0289	1.53	.0282	1.50
5-6	.48	.0198	1.05	.0269	1.43
6-7	.25	.0103	.55	.0244	1.30
7-8	.17	.0071	.38	.0222	1.18
8-9	.48	.0198	1.05	.0220	1.17
9-10	.43	.0178	.95	.0216	1.15
10-11	.72	.0297	1.57	.0223	1.19
11-12	.47	.0194	1.03	.0220	1.17
12-13	.38	.0157	.83	.0216	1.15
13-14	.42	.0174	.93	.0213	1.13
14-15	.80	.0330	1.75	.0220	1.17
15-16	.35	.0144	.77	.0216	1.15
16-17	.05	.0021	.11	.0204	1.09
17-18	.08	.0033	.18	.0195	1.04
18-19	.47	.0194	1.03	.0195	1.04
19-20	.57	.0236	1.25	.0197	1.05
20-21	.58	.0240	1.28	.0199	1.06
21-22	.9	.0372	1.98	.0207	1.10
22-23	.3	.0124	.66	.0203	1.08
23-24	.1	.0041	.22	.0197	1.05
24-25	4.0	.0206	1.09	.0199	1.06
25-26	7.7	.0199	1.06	.0199	1.06
26-27	7.0	.0182	.97	.0195	1.04
27-28	10.9	.0188	1.0	.0193	1.03
28-29	14.6	.0189	1.0	.0192	1.02
29-30	14.0	.0182	.97	.0190	1.01
30-31	18.0	.0187	1.0	.0189	1.01

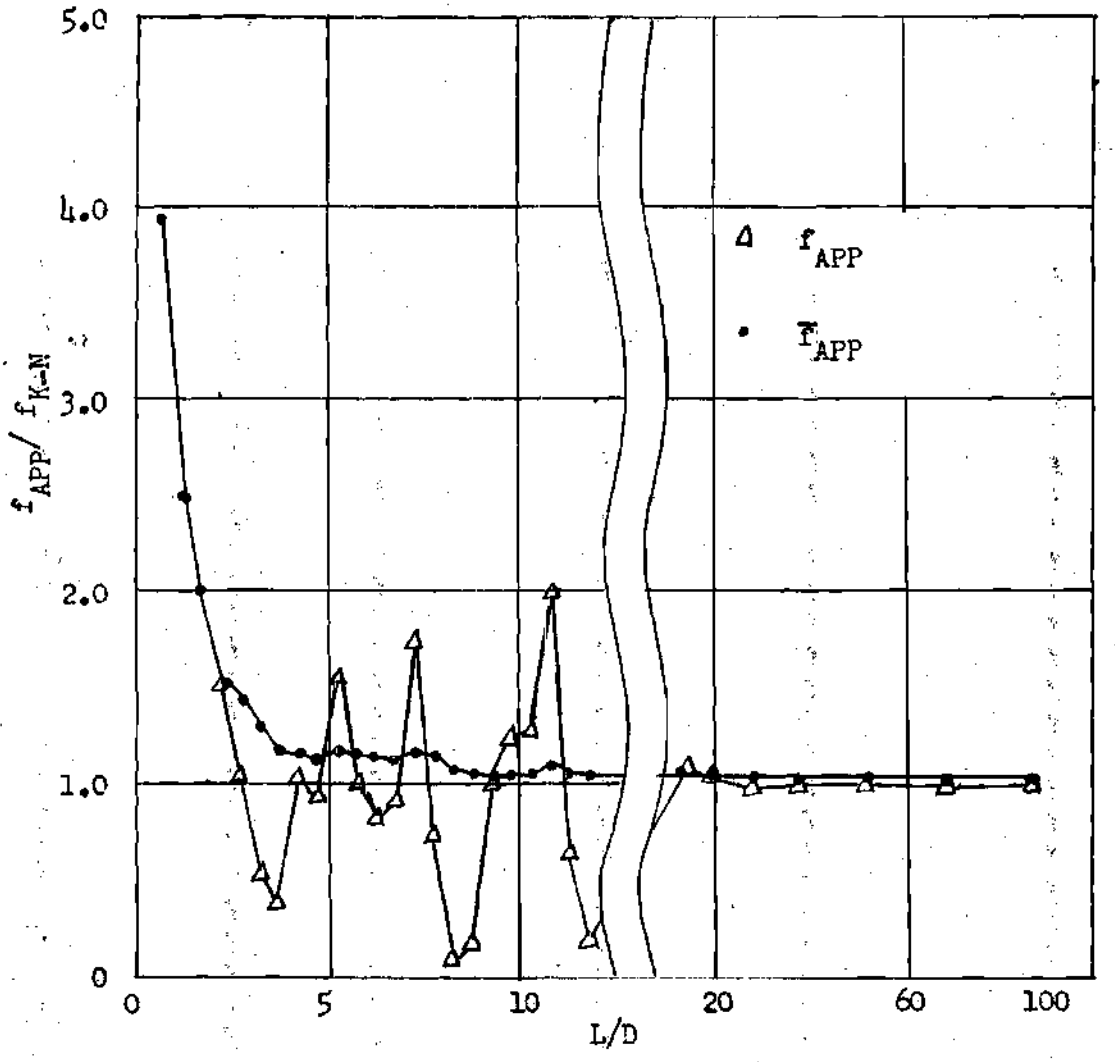

Figure 18. Results for Test D, Entry III. Ratios of local and integrated apparent friction coefficients to the Karman-Nikuradse friction coefficient against L/D for a constant value of R_D.

Table 19. Test E, Entry III

P_{cc} 21 psig

W_w 110½ lbs/min.

T_w 82°

R_D 91,100

f_{K-N} .0183

Pressure Taps	ΔP ($"H_2O$)	f_{APP}	f_{APP}/f_{K-N}	$\bar{f}_{APP}$	$\bar{f}_{APP}/f_{K-N}$
0-1	30.3	.980	53.5	.980	53.5
1-2	+25.5			.0777	4.25
2-3	+ .3			.0485	2.64
3-4	+ .9			.0292	1.59
4-5	.35	.0114	.62	.0256	1.40
5-6	.55	.0178	.97	.0244	1.33
6-7	.6	.0195	1.07	.0235	1.28
7-8	.5	.0162	.89	.0224	1.22
8-9	.6	.0195	1.07	.0222	1.21
9-10	.65	.0211	1.15	.0222	1.21
10-11	.85	.0276	1.51	.0226	1.23
11-12	.3	.0097	.53	.0216	1.18
12-13	.5	.0162	.89	.0212	1.16
13-14	.6	.0195	1.07	.0210	1.15
14-15	.8	.0260	1.42	.0214	1.17
15-16	.65	.0211	1.15	.0214	1.17
16-17	.2	.0065	.36	.0205	1.12
17-18	.25	.0081	.44	.0198	1.08
18-19	.3	.0097	.53	.0193	1.05
19-20	.7	.0227	1.24	.0194	1.06
20-21	.9	.0292	1.60	.0198	1.08
21-22	1.4	.0453	2.48	.0211	1.15
22-23	.3	.0097	.53	.0205	1.12
23-24	.3	.0097	.53	.0202	1.10
24-25	4.7	.0190	1.04	.0200	1.09
25-26	10.1	.0205	1.12	.0200	1.09
26-27	9.0	.0183	1.0	.0196	1.07
27-28	14.1	.0191	1.04	.0194	1.06
28-29	18.7	.0189	1.03	.0193	1.05
29-30	18.3	.0185	1.01	.0191	1.04
30-31	22.2	.0180	.98	.0189	1.03

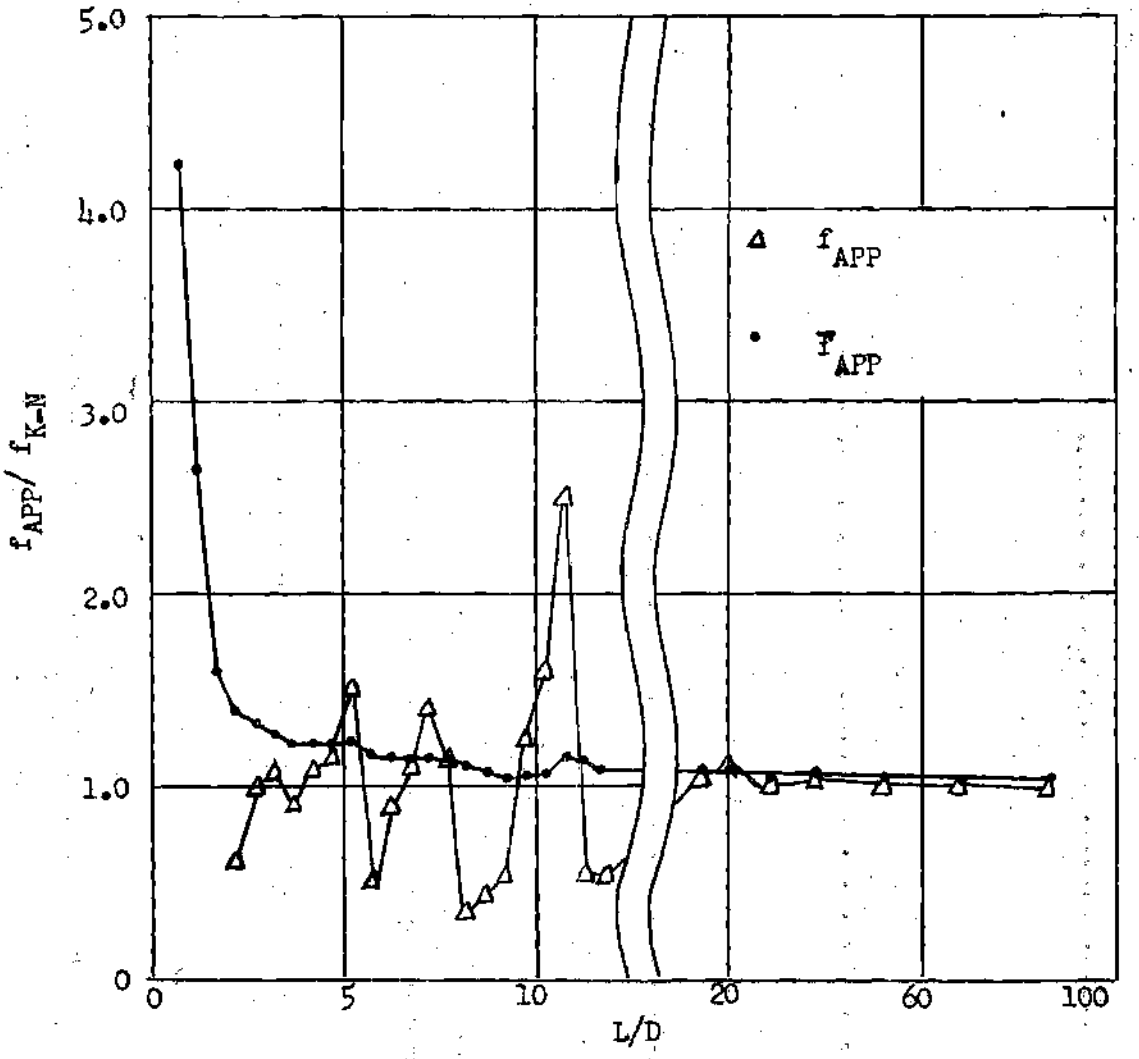

Figure 19. Results for Test E, Entry III. Ratios of local and integrated apparent friction coefficients to the Karman-Nikuradse friction coefficient against L/D for a constant value of R_D.

Table 20. Test F, Entry III

P_{cc}	20 psig	R_D	108,000
W_w	131 lbs/min.	f_{K-N}	.0177
T_w	82°		

Pressure Taps	ΔP ($"H_2O$)	f_{APP}	f_{APP}/f_{K-N}	$\bar{f}_{APP}$	$\bar{f}_{APP}/f_{K-N}$
0-1	19.4	.446	25.4	.446	25.4
1-2	+12.8			.0759	4.28
2-3	+ .35			.0478	2.70
3-4	+ .45			.0333	1.88
4-5	.2	.0046	.26	.0276	1.56
5-6	.4	.0092	.52	.0244	1.38
6-7	.8	.0184	1.04	.0237	1.34
7-8	.7	.0161	.91	.0227	1.28
8-9	.45	.0104	.59	.0213	1.20
9-10	.55	.0127	.72	.0205	1.16
10-11	1.8	.0415	2.35	.0223	1.26
11-12	.4	.0092	.52	.0213	1.20
12-13	.95	.0219	1.24	.0213	1.20
13-14	.75	.0173	.98	.0211	1.19
14-15	.95	.0219	1.24	.0211	1.19
15-16	.8	.0184	1.04	.0209	1.18
16-17	.25	.0057	.32	.0200	1.13
17-18	.55	.0127	.72	.0196	1.11
18-19	.75	.0173	.98	.0195	1.10
19-20	.95	.0219	1.24	.0196	1.11
20-21	.55	.0127	.72	.0193	1.09
21-22	1.5	.0346	1.96	.0200	1.13
22-23	.5	.0115	.65	.0196	1.11
23-24	.3	.0069	.39	.0191	1.08
24-25	6.7	.0192	1.09	.0191	1.08
25-26	12.8	.0184	1.04	.0189	1.07
26-27	13.0	.0187	1.06	.0188	1.06
27-28	18.9	.0181	1.02	.0186	1.05
28-29	24.5	.0177	1.0	.0183	1.04
29-30	24.2	.0174	.99	.0182	1.03
30-31	30.2	.0174	.99	.0180	1.02

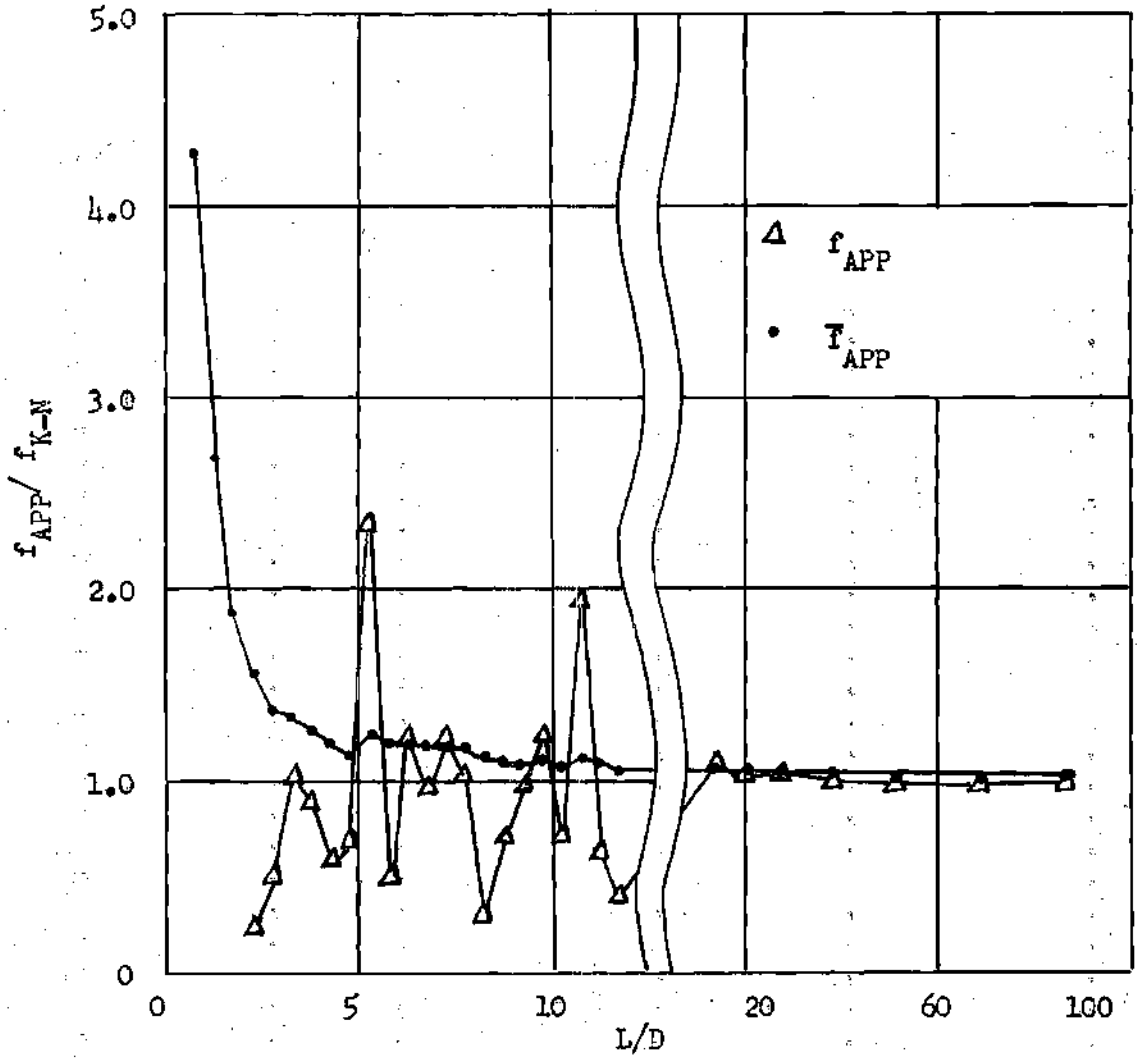

Figure 20. Results for Test F, Entry III. Ratios of local and integrated apparent friction coefficients to the Karman-Nikuradse friction coefficient against L/D for a constant value of R_D.

Table 21. Test G, Entry III

P_{cc}	24 psig	R_D	139,500
W_w	169 lbs/min.	f_{K-N}	.0168
T_w	82°		

Pressure Taps	ΔP ("H_2O)	f_{APP}	f_{APP}/f_{K-N}	$\bar{f}_{APP}$	$\bar{f}_{APP}/f_{K-N}$
0-1	28.8	.401	23.9	.401	23.9
1-2	+20.4			.0585	3.48
2-3	1.3	.0182	1.08	.0451	2.68
3-4	.4	.0056	.33	.0352	2.09
4-5	.2	.0028	.17	.0288	1.71
5-6	1.4	.0195	1.16	.0272	1.62
6-7	.2	.0028	.17	.0236	1.40
7-8	2.1	.0293	1.74	.0244	1.45
8-9	.65	.0098	.58	.0227	1.35
9-10	.85	.0119	.71	.0216	1.28
10-11	1.4	.0195	1.16	.0214	1.27
11-12	1.2	.0168	1.0	.0210	1.25
12-13	.5	.0070	.42	.0199	1.18
13-14	2.1	.0293	1.74	.0206	1.23
14-15	.5	.0070	.42	.0197	1.17
15-16	.4	.0056	.33	.0188	1.12
16-17	1.8	.0251	1.49	.0192	1.14
17-18	1.9	.0265	1.58	.0196	1.16
18-19	1.0	.0140	.84	.0193	1.15
19-20	.6	.0084	.50	.0187	1.11
20-21	.6	.0084	.50	.0183	1.09
21-22	1.7	.0237	1.41	.0186	1.11
22-23	1.1	.0154	.92	.0183	1.09
23-24	.5	.0070	.42	.0179	1.06
24-25	10.0	.0174	1.03	.0178	1.06
25-26	19.9	.0174	1.03	.0176	1.05
26-27	21.3	.0186	1.11	.0176	1.05
27-28	29.0	.0168	1.0	.0176	1.05
28-29	40.0	.0174	1.03	.0175	1.04
29-30	37.5	.0164	.98	.0173	1.03
30-31	49.5	.0173	1.03	.0173	1.03

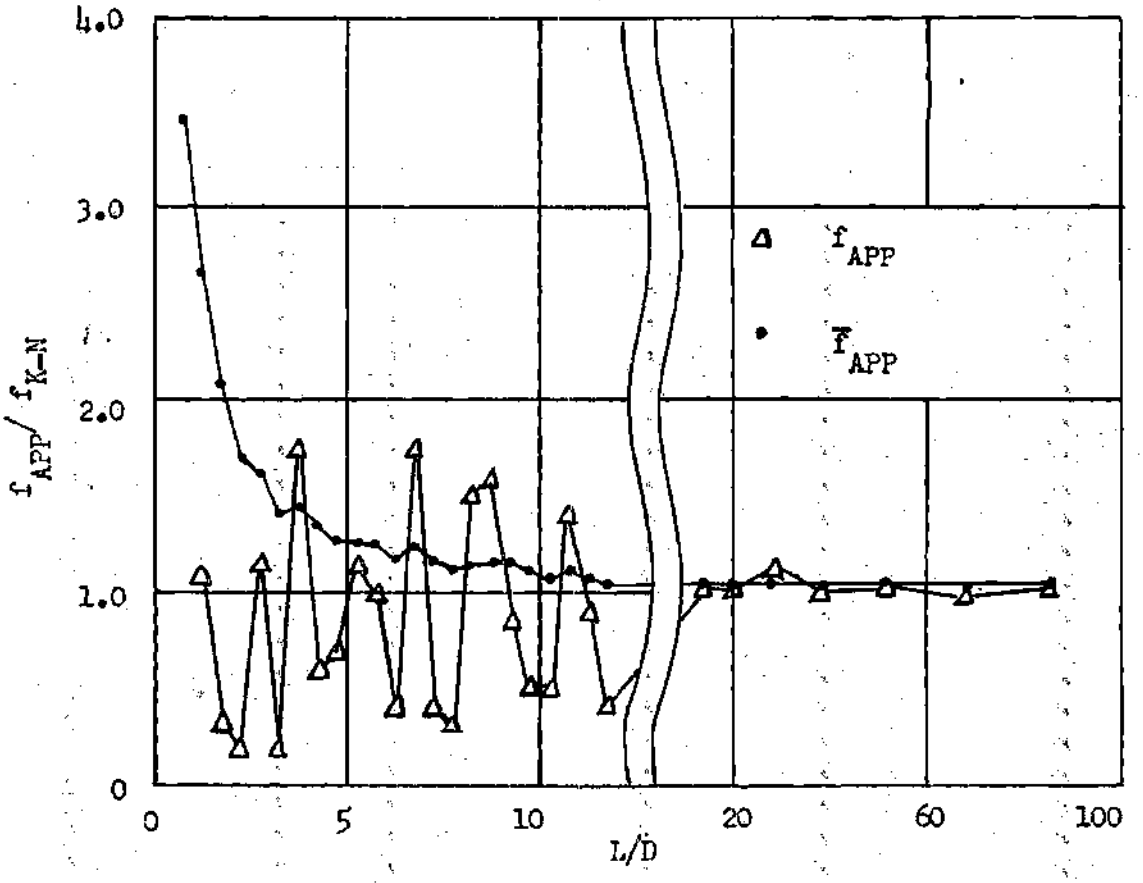

Figure 21. Results for Test G, Entry III. Ratios of local and integrated apparent friction coefficients to the Karman-Nikuradse friction coefficient against L/D for a constant value of R_D.

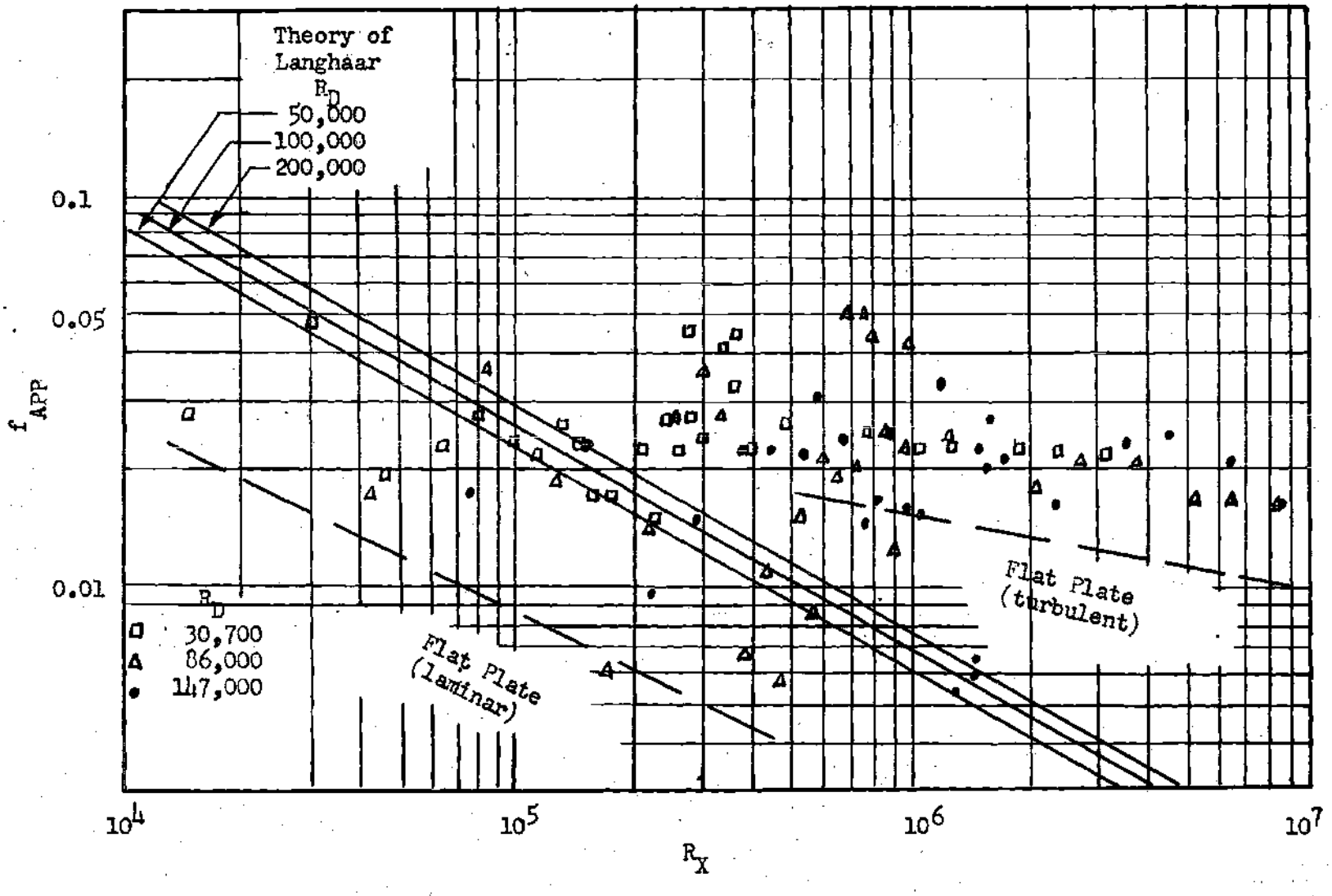

Figure 22. Results for Entry I. Value of f_{APP} against R_X for constant values of R_D. Comparison with flat plate theory and laminar flow theory of Langhaar.

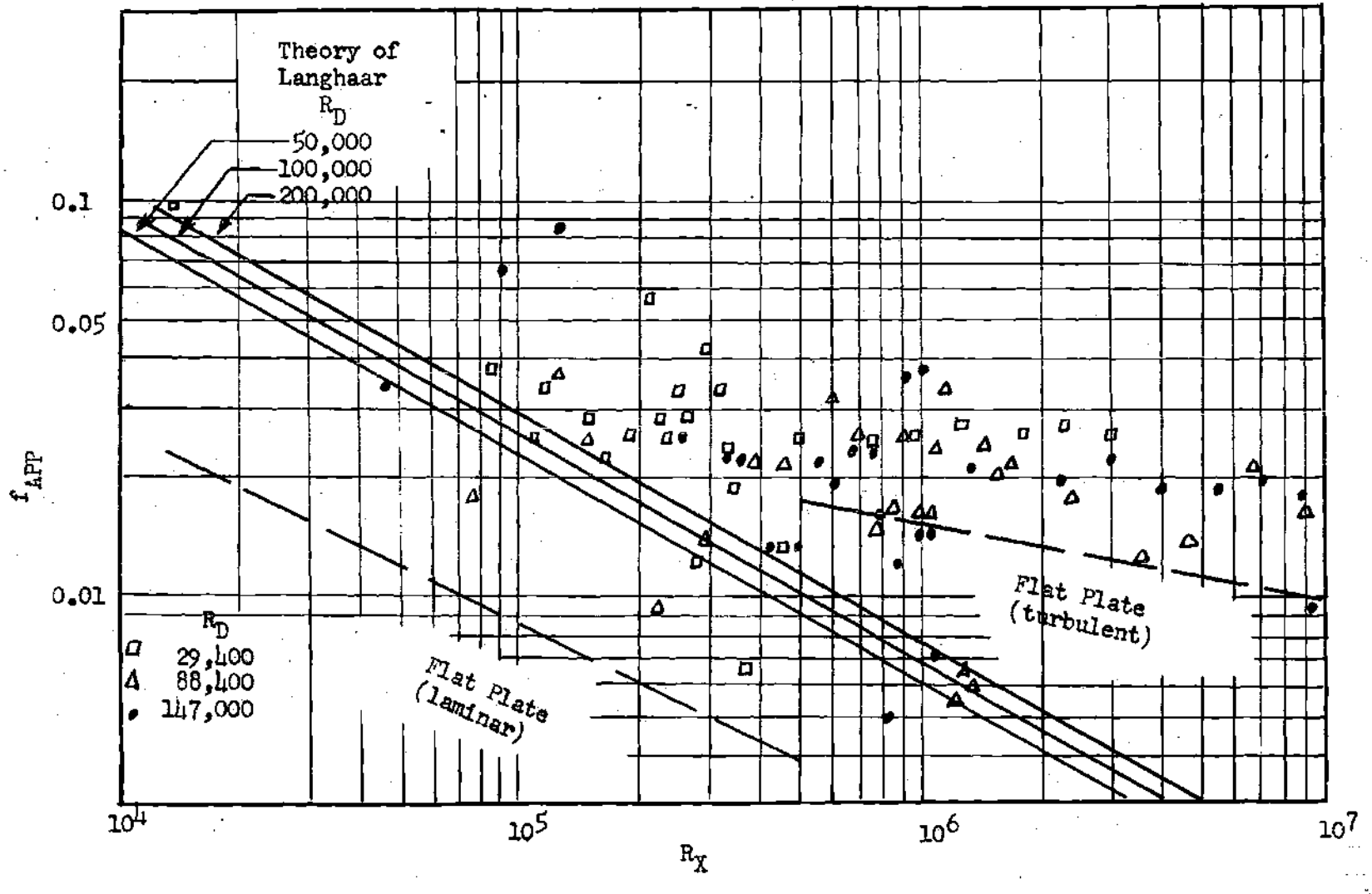

Figure 23. Results for Entry II. Values of f_{APP} against R_X for constant values of R_D. Comparison with flat plate theory and laminar flow theory of Langhaar

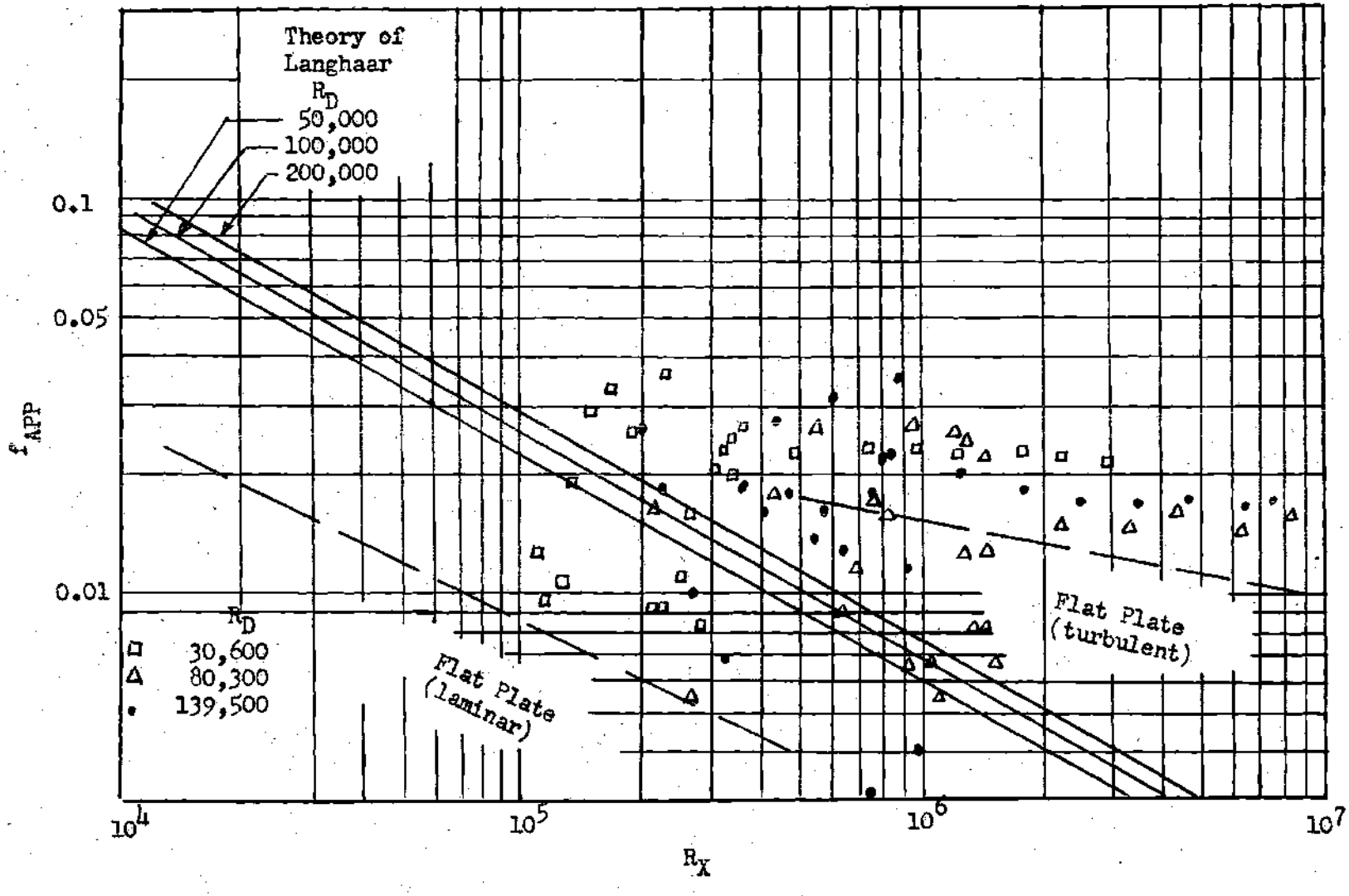

Figure 24. Results for Entry III. Value of f_{APP} against R_X for constant values of R_D. Comparison with flat plate theory and laminar flow theory of Langhaar.

Table 22. Location and Size of Pressure Taps

Tube Diameter 0.545 inches		
Tap	X/D	d
0	0	0.020
1	0.50	0.020
2	1.00	0.020
3	1.50	0.020
4	2.00	0.020
5	2.50	0.020
6	3.00	0.020
7	3.50	0.020
8	4.00	0.020
9	4.50	0.020
10	5.00	0.020
11	5.50	0.020
12	6.00	0.020
13	6.50	0.020
14	7.00	0.020
15	7.50	0.020
16	8.00	0.020
17	8.50	0.020
18	9.00	0.020
19	9.50	0.020
20	10.00	0.020
21	10.50	0.020
22	11.00	0.020
23	11.50	0.020
24	12.00	0.020
25	16.00	0.020
26	24.00	0.020
27	32.00	0.020
28	44.00	0.020
29	60.00	0.020
30	76.00	0.020
31	96.00	0.020

APPENDIX B

METHODS OF CALCULATION

METHODS OF CALCULATION

The Reynolds number based on tube diameter is defined by

$$R_D = VD\rho/\mu$$

where V is the mean velocity in respect to the mass rate of flow and the density and viscosity are evaluated at the mean temperature and pressure of the stream.

The Reynolds number based on distance from the inlet is defined by

$$R_X = VX\rho/\mu$$

where X is the axial distance from the inlet to the point concerned.

The local apparent friction coefficient is defined by

$$p_1 - p_2 = f_{APP} \frac{x_2 - x_1}{D} \frac{V^2}{2g}$$

where p_1 and p_2 are the static pressures, measured at the tube wall, at the axial locations X_1 and X_2 respectively. The value of f_{APP} calculated was taken to be the local value midway between X_1 and X_2. The velocity V is the mean value based on the mass rate of flow.

The integrated apparent friction coefficient at any point X is defined by

$$p_0 - p = \bar{f}_{APP} \frac{X - X_0}{D} \frac{V^2}{2g}$$

where p_0 and p are the static pressures measured at the first pressure tap and point X respectively.

The Karman-Nikuradse coefficient is defined by the relationship

$$\frac{1}{\sqrt{f_{K-N}}} = 2.0 \log_{10} (R_D\sqrt{f_{K-N}}) - 0.8$$

APPENDIX C

APPARATUS

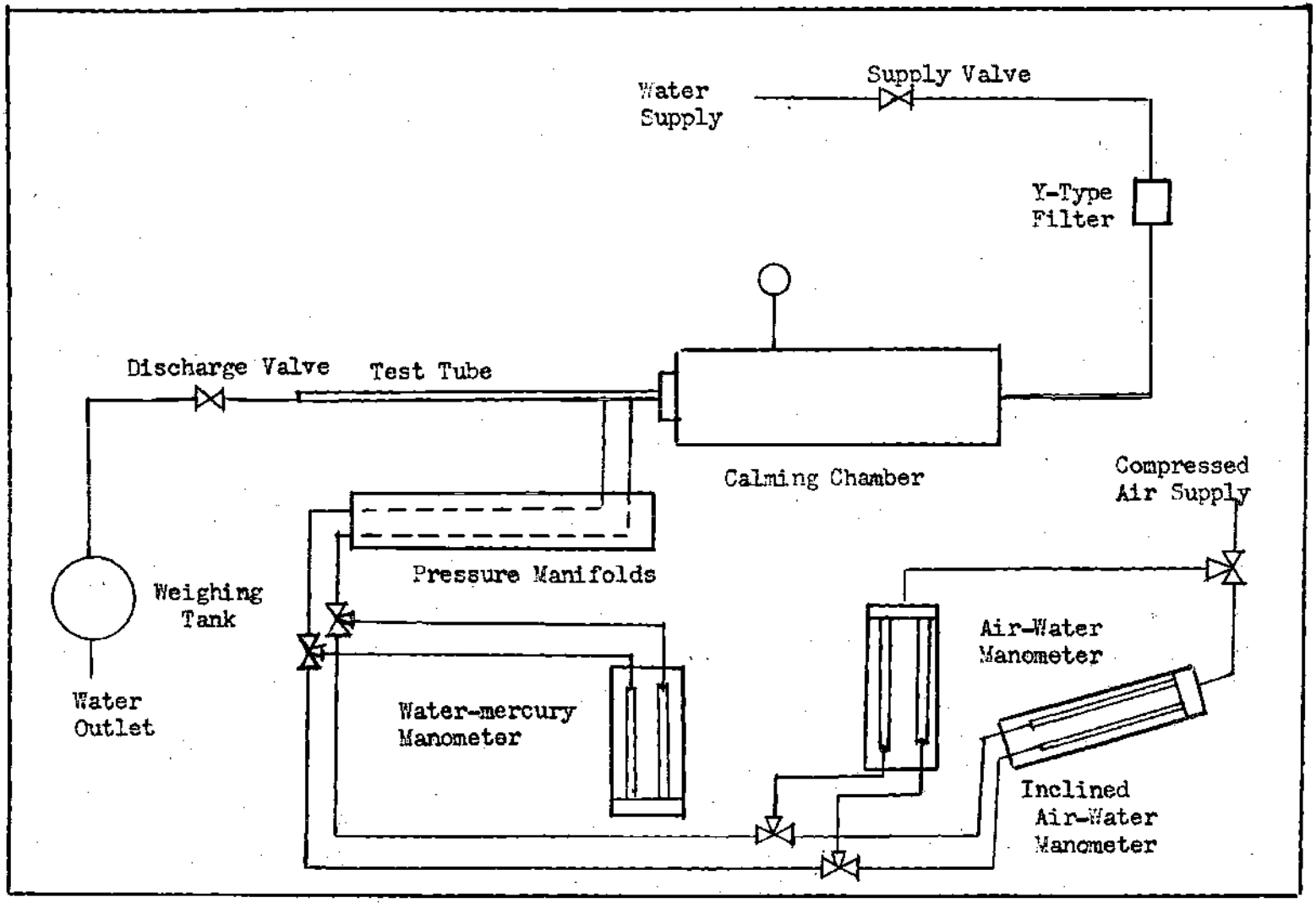

Figure 25. Flow Diagram of Apparatus

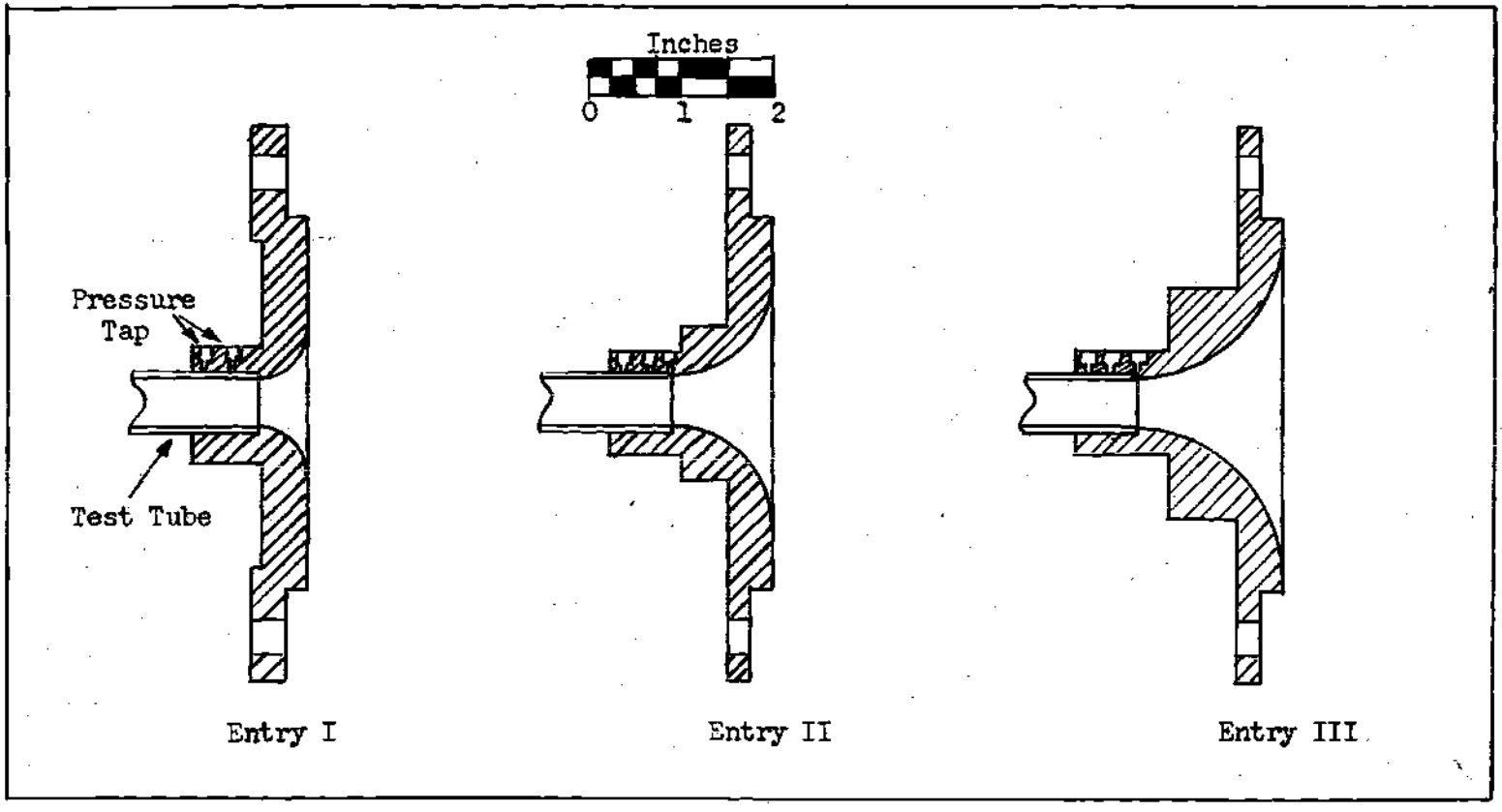

Figure 26. Details of Entry Sections

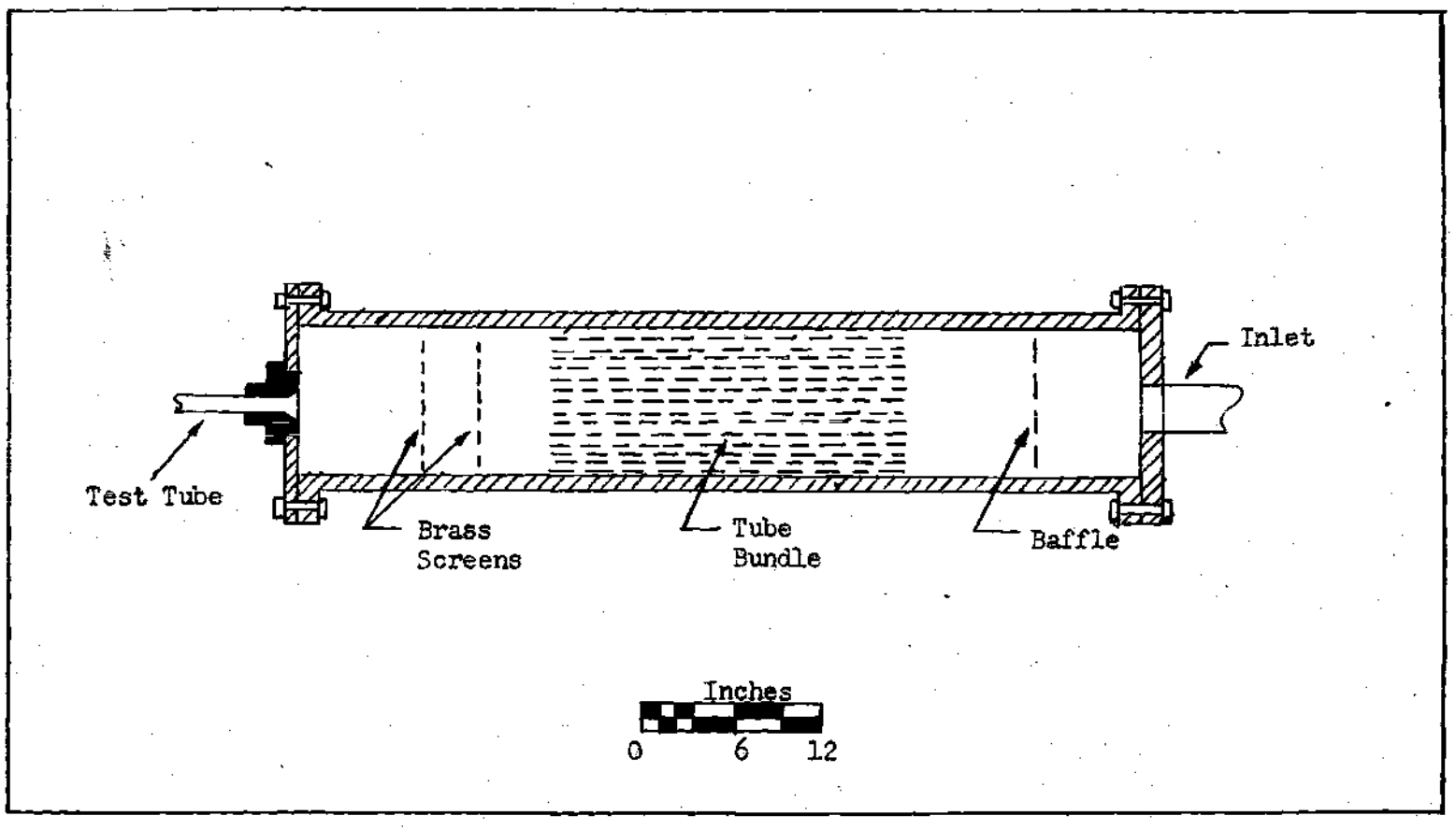

Figure 27. Details of Calming Chamber

BIBLIOGRAPHY

1. Shapiro, A. H., and Smith, R. D., Friction Coefficients in the Inlet Length of Smooth Round Tubes, N.A.C.A. Technical Note #1785, Nov. 1948, p. 3.

2. Loc. cit.

3. Langhaar, H. L., "Steady Flow in the Transaction Length of a Straight Tube," Journal of Applied Mechanics, Vol. 9, June 1942, pp. 55-58.

4. Shapiro and Smith, op. cit., p. 4.

5. Loc. cit.

6. Egli, A., "The Leakage of Gases Through Narrow Channels", Journal of Applied Mechanics, Vol. 4, March 1937, p. 63.

7. Keenan, J. H., and Neuman, E. P., "Measurement of Friction in a Pipe for Subsonic and Supersonic Flow of Air," Journal of Applied Mechanics, Vol. 13, June 1946, pp. 91-100.

8. Shapiro and Smith, op. cit.

9. Huie, W. E., An Investigation of Friction Coefficients in the Inlet Length of Smooth Round Tubes, Thesis, School of Mech. Eng., Ga. Inst. of Tech., Sept. 1953.

10. White, C. M., "Fluid Friction and its Relations to Heat Transfer", Trans. Institution of Chem. Engrs., London, Vol. 10, 1932, p. 66.

11. Aladyev, I. T., Experimental Determination of Local and Mean Coefficients of Heat Transfer for Turbulent Flow in Pipes, Translation, N.A.C.A. Technical Memorandum #1356, Feb. 1954.

12. Boelter, L. M. K., Young, G., and Iverson, H. W., Distribution of Heat Transfer Rate in the Entrance Section of a Circular Tube, N.A.C.A. Technical Note #1451, July 1948.